TrkB activation in Parvalbumin interneurons orchestrates cortical plasticity

Frederike Winkel[1], Mathias B. Voigt[1], Giuliano Didio[1], Salomé Matéo[2], Elias Jetsonen[1], Maria Llach Pou[1], Anna Steinzeig[1], Maria Ryazantseva[3,1], Juliana Harkki[1], Jonas Englund[3,1], Stanislav Khirug[1], Claudio Rivera[1], Satu Palva[1], Tomi Taira[4, 1], Sari E. Lauri[3,1], Juzoh Umemori[1§], Eero Castrén[1]

1 Neuroscience Center, HiLIFE, University of Helsinki, Finland.

2 Master de Neurosciences Moléculaires, Cellulaires et Intégrées Aix-Marseille University

3 Molecular and Integrative Biosciences Research Programme, University of Helsinki, Finland

4 Department of Veterinary Biosciences and Neuroscience Center, University of Helsinki, Finland

§ Corresponding author

Juzoh Umemori,

Neuroscience center, HiLife, University of Helsinki, 00790 Helsinki, Finland

Phone +358-45-1578-930

juzoh.umemori@helsinki.fi

Summary

Critical period plasticity during early postnatal life is followed by a consolidated state through the maturation of interneuron networks and development of perineuronal nets (PNN) surrounding parvalbumin (PV) interneurons. However, critical period-like plasticity can be induced in the adult brain (iPlasticity). Over a shorter time scale, PV interneurons can alternate between high and low plasticity states (PV-plasticity) to regulate memory encoding and consolidation.

We now show that iPlasticity and PV-plasticity in the adult visual cortex are induced by the activation of TrkB neurotrophin receptors in PV interneurons. Optical activation of TrkB specifically in PV interneurons switches adult cortical networks into a state of elevated plasticity within minutes. The activation changes PV properties characterized by ocular dominance plasticity and reduced PV and PNN expression. Our results show that TrkB activity within PV interneurons is essential for iPlasticity and orchestrates plasticity states within adult cortical networks.

42 ## Introduction

43 Neuronal brain plasticity is a key process to adjust maladapted networks but is restricted to critical
44 periods, time windows in which the brain is particularly sensitive to instructive signals (Hensch,
45 2005). Recent work has demonstrated that critical periods can be reopened during adult life by
46 interventions, such as environmental enrichment (Sale et al., 2007) and antidepressant treatment
47 (Karpova et al., 2011; Maya-Vetencourt et al., 2008; Mikics et al., 2018). Chronic treatment with the
48 antidepressant fluoxetine, for example, reinstates ocular dominance plasticity in the adult visual
49 cortex when combined with monocular deprivation (Maya-Vetencourt et al., 2008). We have
50 hypothesized that fluoxetine can induce a critical period-like or juvenile-like plasticity (iPlasticity)
51 through modification of inhibitory and excitatory balance or actions on the inhibitory network
52 (Karpova et al., 2011; Maya-Vetencourt et al., 2008; Umemori et al., 2018).

53 In the visual cortex, the maturation of the GABAergic parvalbumin-expressing (PV) interneuron
54 network promotes the closure of critical periods and restricts ocular dominance plasticity (Huang et
55 al., 1999; Jiang et al., 2010; Pizzorusso et al., 2002) since they control a large repertoire of pyramidal
56 neurons (Hu et al., 2014). During adulthood, external stimuli can switch the configurations of PV
57 interneurons between plastic/immature and consolidated states as defined by low- and high-
58 expressing PV cells, respectively (Donato et al., 2013), here defined as PV-plasticity.

59 The neurotrophic BDNF/TrkB pathway is a crucial modulator of neuronal plasticity. We have
60 previously shown that fluoxetine can activate TrkB receptors by inducing TrkB autophosphorylation,
61 and subsequent downstream signaling, such as phosphorylation of cAMP-related element binding
62 (CREB) protein (Rantamäki et al., 2007). PV interneurons highly express TrkB receptors (Cellerino et
63 al., 1996) and increased BDNF action promotes the onset and closure of critical periods by enhancing

64 the maturation of the PV network (Huang et al., 1999). Also, the expression of PV in visual cortex
65 interneurons depends on neuronal activity and BDNF in early postnatal development (Patz et al.,
66 2004), indicating a substantial role of the BDNF/TrkB pathway in regulating PV cells.

67 While TrkB is expressed in essentially all neurons, BDNF is not expressed in interneurons. BDNF as a
68 secreted ligand can simultaneously act on several cell types, therefore, it is not clear which neurons
69 mediate the effects of BDNF on plasticity. Here, we show that optically activatable TrkB (optoTrkB)
70 (Chang et al., 2014; Fenno et al., 2014) specifically expressed in PV interneurons of the visual cortex
71 rapidly orchestrates cortical network plasticity. OptoTrkB activation reduced the intrinsic excitability
72 of PV cells through increased phosphorylation of Kv3.1 channels and decreased expression of
73 glutamate receptor subunits resulting in disinhibition of layer II/III pyramidal neurons and permissive
74 visual cortex plasticity when combined with monocular deprivation. Moreover, we observed that
75 TrkB activation in PV interneurons regulates PV and PNN configuration states, resetting the neuronal
76 network into a plastic, immature-like state. Conversely, deleting TrkB from PV interneurons blocked
77 these effects when induced pharmacologically using fluoxetine treatment. These findings
78 demonstrate that TrkB activation in PV interneurons rapidly orchestrates cortical network plasticity
79 and provides new evidence that TrkB receptors are fundamental regulators of intracortical inhibition
80 and plasticity modes during adulthood.

81

82

83

84 # Results

85 **TrkB activation in PV interneurons induces iPlasticity**

86 We hypothesized that TrkB activation in PV interneurons might regulate PV-plasticity as well as
87 iPlasticity. Using a standard protocol for monocular deprivation (MD) and *in vivo* imaging of intrinsic
88 optical signals (IOS) we found that chronic fluoxetine treatment induced a shift of ocular dominance
89 in combination with MD in the adult primary visual cortex (V1) of wild-type mice (WT), but no
90 induction was seen in heterozygous mice with PV-specific conditional TrkB knockout (hPV-TrkB CKO)
91 (Fig. 1A and 1B). These results indicate that iPlasticity induced by fluoxetine is dependent on TrkB
92 activity within PV interneurons.

93 As TrkB receptors are expressed in essentially all neurons, BDNF cannot be used to study cell type-
94 specific functions of TrkB. To specifically activate TrkB in PV interneurons, we used an optically
95 activatable TrkB (optoTrkB) where addition of a plant-derived photolyase homology region (PHR)
96 domain into the C-terminus of full-length TrkB mediates light-induced dimerization of TrkB
97 monomers (Chang et al., 2014) (Fig. 1C) (Figure S1A). Acute light activation of optoTrkB in V1
98 resulted in increased phosphorylation of TrkB and CREB (Figure S2A-S2E). We infected the V1 of
99 adult PV-cre mice with a lentivirus expressing a double-floxed inverted open reading frame of opto-
100 TrkB (DIO-optoTrkB) to specifically express optoTrkB in PV interneurons (Figure S1B). When V1 was
101 stimulated twice daily by light through a transparent skull (Steinzeig et al., 2017) for 30 seconds (Fig.
102 1D) during 7 days of MD, we observed a shift in ocular dominance index (ODI) towards the non-
103 deprived ipsilateral eye, while mice infected with optoTrkB but not exposed to light showed no
104 change in their ODI (Fig.1E). The shift persisted for a week in the absence of visual deprivation or
105 light stimulation (Fig. 1E). When we then closed the eye that had been left open during the first MD
106 session and again exposed the cortex to light twice daily for 7 days, we again observed a shift towards

107 the non-deprived eye (Fig. 1E). Light stimulation alone during 7 days of MD had no effect on visual
108 cortex plasticity in PV-cre mice without optoTrkB expression (Figure S2F). Thus, the activation of TrkB
109 in PV interneurons is necessary and sufficient for iPlasticity.

110 **TrkB in PV cell enhances network activity**

111 A shift in ocular dominance takes several days to occur. To test how fast TrkB activation in PV
112 interneurons regulates plasticity, we studied the induction of long-term potentiation (LTP). LTP
113 occurrence through theta-burst stimulation (TBS) in V1 is restricted to critical periods (Kirkwood et
114 al., 1996). TBS stimulation (Kirkwood & Bear, 1994) of acute V1 slices expressing optoTrkB in PV
115 interneurons did not induce LTP in slices kept in darkness, but robust LTP was induced in slices
116 exposed for 30 seconds to blue light 30 minutes before the TBS stimulation (Fig.2A). Chronic
117 fluoxetine treatment also permitted LTP induction after TBS stimulation, as previously reported
118 (Maya-Vetencourt et al., 2008), but this effect was absent in hPV-TrkB CKO mice (Fig. 2B). These
119 results demonstrate that TrkB activation in PV interneurons rapidly enhances synaptic plasticity in
120 V1 and is necessary for fluoxetine-induced effects.

121 Plasticity in the visual cortex is controlled locally by synchronized neuronal oscillations that are
122 regulated by the activity of PV interneurons (Galuske et al., 2019; Lee et al., 2012). *In vivo* local field
123 potential (LFP) recordings of neuronal activity from V1 revealed a progressive increase in the
124 broadband (4–112 Hz) LFP power in response to a 30-second long optoTrkB activation (Fig. 2C). The
125 broadband magnitude at 100 minutes after stimulation showed a significant increase when
126 compared to the pre-stimulation baseline. Furthermore, no increase in the broadband magnitude
127 was observed in optoTrkB infected control animals stimulated with infrared light (780nm) (Fig. 2D).
128 We also found increases in the magnitude at the separate frequency bands, particularly in α and γ
129 range at 100 minutes after optoTrkB activation (Fig. 2E). These results suggest that optoTrkB

130 activation in PV interneurons promotes synchronized oscillations, which renders the network state
131 of the visual cortex responsive and permissive for plasticity.

132

133 **TrkB activation in PV interneurons reduces cell excitability**

134 To identify the TrkB-dependent intrinsic changes of PV interneurons underlying increased plasticity,
135 we obtained patch clamp recordings from optoTrkB-positive PV interneurons in the V1 co-expressing
136 TdTomato (Figure S1C and S1D). OptoTrkB was activated 30-60 minutes before the recordings using
137 a 30-second light stimulation. The intrinsic excitability of PV cells in optoTrkB stimulated slices was
138 significantly lower when compared to the non-activated controls (Fig. 3A and 3F) (Table S1A), and
139 was accompanied by trends towards increased action potential (AP) half-width (Fig. 3B and 3F). We
140 further found that the frequency of spontaneous excitatory postsynaptic currents (sEPSCs) was
141 lower in optoTrkB activated PV interneurons than in controls (Fig. 3C and 3F), indicating changes in
142 excitatory transmission onto PV interneurons. Neither the sEPSC amplitudes nor the frequency or
143 amplitudes of spontaneous inhibitory postsynaptic currents (sIPSC) were changed (data not shown),
144 suggesting that optoTrkB activation specifically affects excitatory inputs. Similar changes in intrinsic
145 excitability (Fig. 4A and 4D) (Table S1B) and AP half-width (Fig. 4B and 4D) were found in PV
146 interneurons after chronic fluoxetine treatment in WT mice, but not in hPV-TrkB CKO mice, although
147 the decrease in sEPSC frequency did not reach statistical significance ($p = 0.5397$) (Fig. 4C and 4D).

148 A decrease in the intrinsic excitability of PV interneurons is likely mediated by changes in potassium
149 currents; it is known that particularly Kv3 channels, which are highly expressed in cortical PV
150 interneurons, regulate the fast-spiking properties (Chow et al., 1999; Du et al., 1996). Kv3.1 channels
151 are directly inhibited by phosphorylation through PKC (Song & Kaczmarek, 2006), a downstream

152 target of TrkB signaling. It is known that chronic fluoxetine treatment promotes Kv3.1 channel
153 phosphorylation (Sagi et al., 2019). We therefore tested whether optoTrkB activation could result in
154 enhanced phosphorylation of Kv3.1 channels by immunohistochemically examining the expression
155 intensities of phospho-Kv3.1 within PV interneurons. Indeed, optoTrkB activation (twice daily, 7 days)
156 resulted in increased phospho-Kv3.1 expression in PV interneurons in visual cortical slices (Fig. 3D
157 and 3E), suggesting that optoTrkB activation can inhibit these channels through phosphorylation,
158 thereby directly mediating the intrinsic excitability of PV interneurons.

159

160 **TrkB regulates plasticity-related genes in PV interneurons**

161 To further identify the molecular mechanisms regulated by TrkB activation in PV interneurons, we
162 performed single nuclei RNA sequencing (snRNA-seq) of visual cortical samples from DIO-optoTrkB-
163 TdTomato-transfected PV-cre mice 60 minutes after a 30-second light stimulation (Figure S3A).
164 Single cell RNA sequencing was not feasible due to potential light-induced optoTrkB activation during
165 cell extraction and processing (Figure S3B). Integrated data analysis (see STAR Methods) identified
166 18 clusters of neurons, including a cluster containing PV interneurons (Fig. 5A; Figure S4 and S5;
167 Table S3 and S4), which was further divided into four PV interneuron clusters using PCA analysis (Fig.
168 5B and 5C; Figure S6 and S7; Table S5). *Arc*, a known downstream signal of TrkB (Messaoudi et al.,
169 2002, 2007; Yin et al., 2002; Ying et al., 2002), was only up-regulated in PV cluster 3 of the light-
170 stimulated group, along with other immediate early genes, such as, *Jun* and *Egr1* (Fig. 5E), indicating
171 that this cluster harbours optoTrkB transfected PV cells. In this cluster, genes related to dendrite
172 morphogenesis, synaptic plasticity, and regulation of excitatory postsynaptic currents were
173 differentially regulated in the light-exposed group (Fig. 5D) (Table S6). Among them, we found a
174 decrease in PV expression (Fig. 5E), and this decrease was confirmed by qPCR (Figure S10).

175 Particularly interesting is the downregulation of *Grin1* and *Grik3* that code for subunits of NMDA and
176 kainate receptors, respectively, essential components of excitatory synapses (Fig. 5E). Knocking out
177 *Grin1* in PV interneurons enhances network oscillations, particularly theta and gamma frequencies
178 (Korotkova et al., 2010). The specific function of the *Grik3* subunit is not fully characterized, but
179 kainate receptors have been shown to regulate both the maturation and excitability of GABAergic
180 interneurons (Jack et al., 2019; Segerstråle et al., 2010), as well as the generation of synchronized
181 activity at the level of neuronal networks (Bartos et al., 2007). As both NMDA and kainate receptors
182 are known to mediate and modulate excitatory synaptic transmission, the downregulation of *Grin1*
183 and *Grik3* might also contribute to the decrease in the intrinsic excitability and sEPSC frequencies
184 (Zhang et al., 2013). In addition, we observed a decrease of *Homeobox protein cut-like 2* (*Cux2*) (fold
185 value, 0.63, Table S6), deletion of which reduces the amplitude and lowers the frequency of mEPSC
186 (Cubelos et al., 2010). Furthermore, *Leucine Rich Repeat And Ig Domain Containing 2* (*Lingo-2*) that
187 is broadly expressed in neurons was reduced after optoTrkB activation (fold value, 0.46, Table S6),
188 and the *Lingo* family members act as negative regulators of TrkB signalling (Meabon et al., 2016) .
189 Those results suggest a novel mechanism through which TrkB activation in PV interneurons rapidly
190 regulates the intrinsic properties of these cells resulting in increased excitatory transmission of the
191 cortical network.

192

193 **TrkB activation regulates PV-plasticity**

194 Upon closure of critical periods, PV interneurons become enwrapped by perineuronal nets (PNN)
195 (Jiang et al., 2005) and PNN removal during adulthood reinstates a juvenile-like plasticity and
196 reduces intracortical inhibition (Lensjø et al., 2017; Pizzorusso et al., 2002). Furthermore, PV
197 expression itself is plastic and regulated by experience (Donato et al., 2013; Karunakaran et al., 2016),

198 low PV expression being associated with plastic and high PV with consolidated networks. Activation
199 of optoTrkB in the V1 PV interneurons for 30 seconds twice daily for 7 days reduced the numbers of
200 PNN-positive (PNN^+), PV/PNN-double-positive (PV^+PNN^+) cells, and PV^+PNN^+ cells within the PV
201 population (Fig. 6A-6D). PV intensities were particularly reduced in the subgroup of PV interneurons
202 expressing high levels of PV (Fig. 6 E, F) and the PNN intensity was reduced in the same high-PV
203 subgroup (Fig. 6G).

204 Similarly, chronic fluoxetine treatment reduced PNN^+ abundance within the PV population in WT,
205 but not in hPV-TrkB CKO mice (Fig. 7A-7C). In addition, PV and PNN intensities were decreased
206 among the high-PV expressing population after fluoxetine treatment in WT but not in hPV-TrkB CKO
207 mice (Fig. 7D and 7E). These results demonstrate that TrkB activation in PV interneurons in the adult
208 V1 induces a plastic network state with low PV and PNN expression.

209

210

211

212 # Discussion

213 Our data demonstrate that TrkB activation in PV interneurons reduces PV interneuron excitability
214 and regulates expression of PV and PNNs, in a manner that resembles PV plasticity in the
215 hippocampus. We propose a converging mechanism that connects PV plasticity and the induction of
216 critical period-like plasticity and show that TrkB activation in PV interneurons orchestrates the
217 plasticity states of cortical networks to allow better encoding of environmental experiences.

218

219 **TrkB activation in PV interneurons as mediators of iPlasticity**

220 We previously demonstrated that chronic fluoxetine treatment can reactivate ocular dominance
221 plasticity in the adult visual cortex (Maya-Vetencourt et al., 2008). This effect was accompanied by
222 a reduction in intracortical GABAergic transmission as measured by decreased extracellular basal
223 GABA levels; induction of LTP after TBS stimulation and increased BDNF protein levels, strongly
224 suggesting a regulatory role of intracortical inhibition in adult visual cortex plasticity (Maya-
225 Vetencourt et al., 2008). Although PV interneurons cover only a small percentage of the total
226 neuronal population, their extensive axonal arborization enable strong inhibitory control over
227 pyramidal cells. As BDNF promotes the maturation of those cells during critical periods, we
228 hypothesized that TrkB activation in PV interneurons could also affect plasticity processes during
229 adulthood. Considering that BDNF and fluoxetine activate TrkB receptors expressed in essentially all
230 neurons, we developed a cre-dependent optoTrkB to circumvent this problem and be able to
231 specifically activate TrkB signaling in PV interneurons only. Strikingly, while BDNF-induced TrkB
232 activation during critical periods promotes the maturation of PV interneurons, thereby restricting
233 visual cortex plasticity, TrkB activation in PV interneurons during adulthood reinstates a critical

234 period-like plasticity machinery through rejuvenating these interneurons. These findings suggest
235 that the plasticity machinery remains intact in the adult brain but needs the right tools to be
236 reactivated.

237

238 **Differential effects of TrkB activation in pyramidal neurons and interneurons?**

239 Reactivation of critical period-like plasticity in the adult brain is associated with reduced cortical
240 inhibition and subsequent disinhibition of cortical networks (Hensch, 2005). BDNF has been shown
241 to strongly promote neuronal activity, excitability (Figurov et al., 1995; Levine et al., 1995, 1998) and
242 LTP (Kang & Schuman, 1995) in hippocampal and cortical excitatory neurons. In contrast, we found
243 that optical activation of TrkB specifically in PV interneurons decreases excitability in PV cells and
244 promotes field LTP in the visual cortex, indicating an increase in network-wide excitatory
245 transmission and dynamics. These findings suggest that activation of TrkB produces differential
246 effects on the cell excitability, increasing and decreasing it in pyramidal neurons and interneurons,
247 respectively. Importantly, however, from the point of view of cortical networks, these differential
248 effects on excitability cooperatively drive increased network activity, through enhanced excitability
249 of pyramidal neurons and reduced activity of inhibitory neurons.

250

251 **Activation of TrkB mediates intrinsic changes in PV interneurons to enhance excitatory**
252 **transmission in the visual cortex**

253 The hallmark of PV interneurons is their high-frequency firing, which is enabled by the high
254 expression of voltage-gated Kv3 channels (Chow et al., 1999; Hu et al., 2014). Kv3 channels are

255 characterized by their fast deactivation during membrane repolarization enabling sustained high-
256 frequency firing. A decrease in their expression as well as their inhibition through PKC
257 phosphorylation is known to reduce cell excitability (Rudy et al., 1999; Song & Kaczmarek, 2006).
258 PKC is a downstream target of TrkB signaling and our data show that TrkB activation in PV
259 interneurons results in enhanced phosphorylation of Kv3.1 channels, demonstrating control of TrkB
260 signaling over PV intrinsic excitability. The decreased firing frequency of PV cells in turn enhances
261 excitatory transmission necessary for visual cortex plasticity. The maturation of PV cells throughout
262 critical period is concurrent with an increase in the fast-spiking firing frequency and an increase in
263 Kv3.1 expression (Du et al., 1996; Plotkin et al., 2005). The upregulation of these channels therefore
264 likely contributes to the maturation of PV interneurons, closure of critical periods and restricted
265 visual cortex plasticity during adulthood. Interestingly, the fast-spiking phenotype of PV
266 interneurons fails to develop in BDNF null mice (Itami et al., 2007). Considering that Kv3.1 channels
267 are specifically expressed in high-frequency firing neurons, this could account for the differential
268 effects of TrkB actions in pyramidal cells and PV interneurons.

269

270 **Activation of optoTrkB regulates PV plasticity**

271 Exciting research suggests that PV interneurons show intrinsic plasticity and can change between
272 high and low plasticity states when exposed to different environmental conditions (Donato et al.,
273 2013). For example, environmental enrichment that is known to promote neuronal plasticity,
274 induces a low PV-expressing network state. In contrast, contextual fear conditioning that is
275 associated with network consolidation, shifts the PV network into a high-PV expressing state (Donato
276 et al., 2013). Additionally, PV expression progressively increases throughout development and could
277 therefore also account for the reduction in brain plasticity during adulthood (Donato et al., 2013;

278 Umemori et al., 2015). Interestingly, TrkB activation in PV interneurons can regulate PV plasticity
279 states, and this effect may be mediated through direct regulation of PV mRNA expression as
280 confirmed by single nuclei sequencing and qPCR. As PV is a Ca^{2+} buffer, a low PV expressing state
281 could directly regulate PV interneuron firing (Eggermann & Jonas, 2012; Hu et al., 2014)

282 In the hippocampus, PV cell intensity is generally higher when enwrapped by PNNs and PV cells with
283 weak staining intensity often lack PNNs (Yamada et al., 2015). The maturation of the PV network is
284 associated with the formation of PNNs (Pizzorusso et al., 2002) and enzymatic digestion of PNNs can
285 restore plasticity in adulthood (Lensjø et al., 2017; Pizzorusso et al., 2002) and results in a decrease
286 in PV intensity and PV mRNA levels, suggesting a correlation between PNN expression and PV
287 configuration states (Yamada et al., 2015). In fact, a recent study by Devienne et al. demonstrates
288 that transient electrical silencing of visual cortical PV interneurons induces a regression of PNN
289 (Devienne et al., 2019), indicating a causal relationship between PV activity and the accumulation of
290 PNNs.

291 In conclusion, we show that activation of TrkB receptors in PV interneurons rapidly reduces their
292 excitability, thereby changing cortical network dynamics to promote iPlasticity. We further show
293 that iPlasticity induced by fluoxetine requires TrkB activation in PV interneurons. These results
294 suggest that TrkB activity in PV cells dynamically controls the plasticity states of cortical networks to
295 regulate network rewiring, learning and consolidation. These mechanisms might be extrapolated to
296 other brain areas and therefore aids in the understanding of the pathophysiology of neuropsychiatric
297 disorders and the rational design of clinical interventions.

298

Acknowledgments

We thank our lab technicians Sulo Kolehmainen and Outi Nikkilä for technical and practical help to realize the experiments. We also thank the animal caretakers in the Laboratory Animal Center of the University of Helsinki (UH) for help and support with the animals, and Louisa Böttcher, Mirko Torheiden and Marvin Krampe for their help with the Western Blots. We also thank Noora Aarnio and Nina M Peitsaro in the Biomedicum Flow cytometry unit for helping FACS, and Jenni Lahtela and Bshwa Ghimire in FIMM Single Cell Analytics core facility supported by UH and Biocenter Finland. In addition, we are grateful to Eija Korpelainen and Maria Lehtivaara in CSC for helping to run Chipster. Castrén lab was supported by the ERC grant # 322742 – iPLASTICITY, the Sigrid Jusélius foundation, Jane & Aatos Erkko Foundation, Academy of Finland grants #294710 and #307416, EU Joint Programme - Neurodegenerative Disease Research (JPND) *CircProt* project co-funded by EU and Academy of Finland #643417, the doctoral program Brain&Mind and the bilateral exchange program between Academy of Finland and JSPS (Japan Society for the Promotion of Science).

Declaration of conflicting interests

EC has received a lecturer fee from Jansen Cilac.

Author contributions

F.W., J.U. and E.C. conceived and designed the project. F.W. performed the experiments. M.V. analyzed the in vivo electrophysiology recordings under the supervision of S.P.. G.D. helped with the Western Blot experiments. M.L. cut the brains on the vibratome and helped with immunohistochemistry. E.J., S.M., and J.U. helped with single nuclei sequencing experiments and

data analysis. A.S. helped with the behavioral experiment using hPV-TrkB CKO mice combined with fluoxetine treatment. J.H. analyzed the PV/PNN intensities. S.K., C.R., J.E., M.R., S.K., T.T. and S.L. provided supervision and support during the electrophysiological experiments. F.W., J.U. and E.C. wrote the manuscript.

Figures

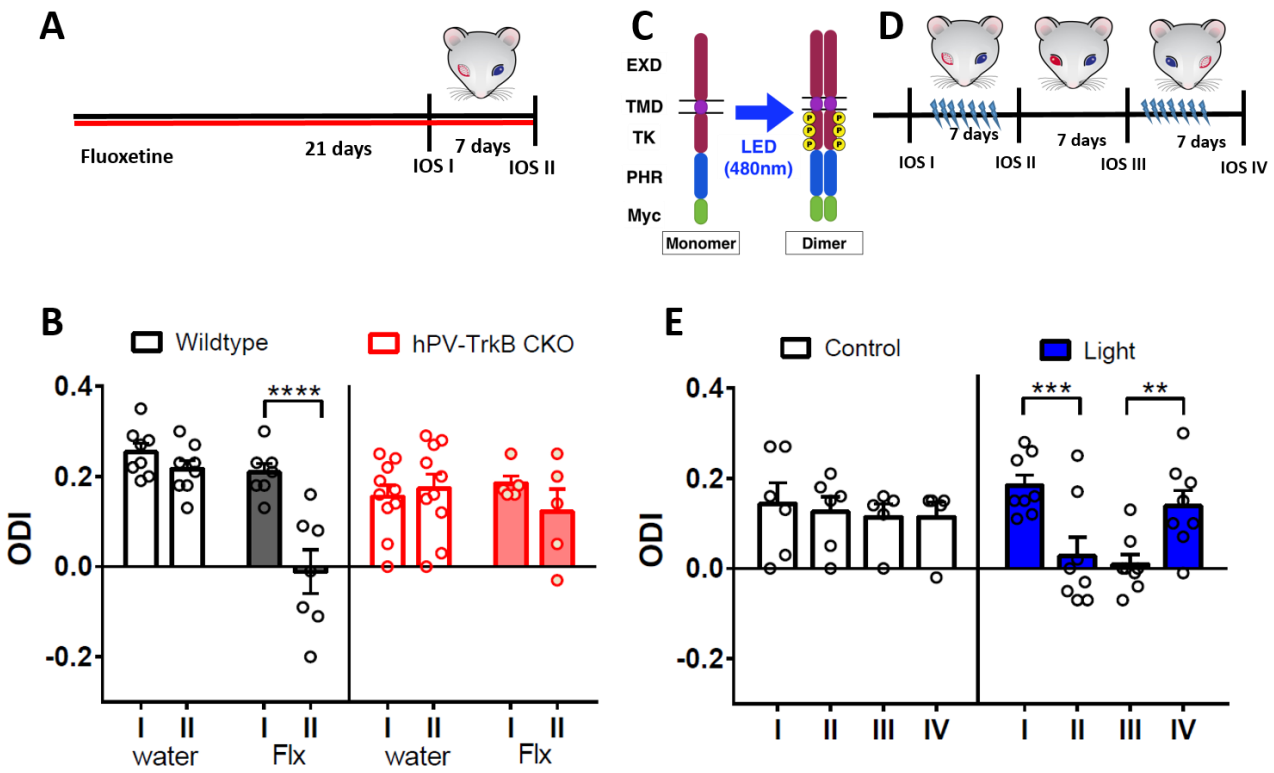

Fig. 1 TrkB activation in PV interneurons induces iPlasticity

(A) Experimental timeline for the shift in ocular dominance paradigm with hPV-TrkB CKO mice treated chronically with Fluoxetine (Flx).

(B) ODI after chronic Flx treatment in WT and hPV-TrkB CKO mice. Flx permits MD to shift the ODI towards the non-deprived eye in the V1 of WT mice, but fails to do so in hPV-TrkB CKO mice. Two-way ANOVA with Sidak's post-hoc test comparing the ODI of IOS I and II. WT water, $p = 0.7311$; WT Flx $p < 0.0001$; CKO water, $p = 0.9621$; CKO Flx, $p = 0.5048$. n = 5 – 10 animals/group.

(C) Structure of optoTrkB conjugated to a light reactive PHR domain, which dimerizes optoTrkB upon blue light exposure.

(D) Experimental timeline of the shift in ocular dominance paradigm with optoTrkB. OptoTrkB was stimulated with blue light twice daily (30 seconds) for 7 days during MD.

(E) MD of the contralateral eye induces a shift in ocular dominance when combined with stimulation of optoTrkB (IOS I-II) (n = 6-8 animals/group). Two-way ANOVA with Sidak's post-hoc test comparing the ODI of IOSI and II (control, $p = 0.9094$; light, $p = 0.001$). The shift is preserved if the eyes are not deprived (IOS II-III). Two-way ANOVA with Sidak's post-hoc comparing the ODI of IOS II with III (control, $p = 0.4985$; light, $p = 0.6915$). Stimulation of optoTrkB reverses shift in ocular dominance when combined with MD of the ipsilateral eye (IOS III-IV) (n = 6-7 animals/group; one mouse excluded due to corneal infection). Two-way ANOVA with Sidak's post-hoc test comparing ODI of IOS III and IV (control, $p = 0.9094$; light, $p = 0.001$). Flx, fluoxetine; ODI, ocular dominance index; MD, monocular deprivation; V1, primary visual cortex; PHR, photolyase homology region; EXD, extracellular domain; TMD, transmembrane domain; TK, tyrosine kinase domain. Bars represent means ± SEM. ** $p < 0.01$*** $p < 0.001$; **** $p < 0.0001$

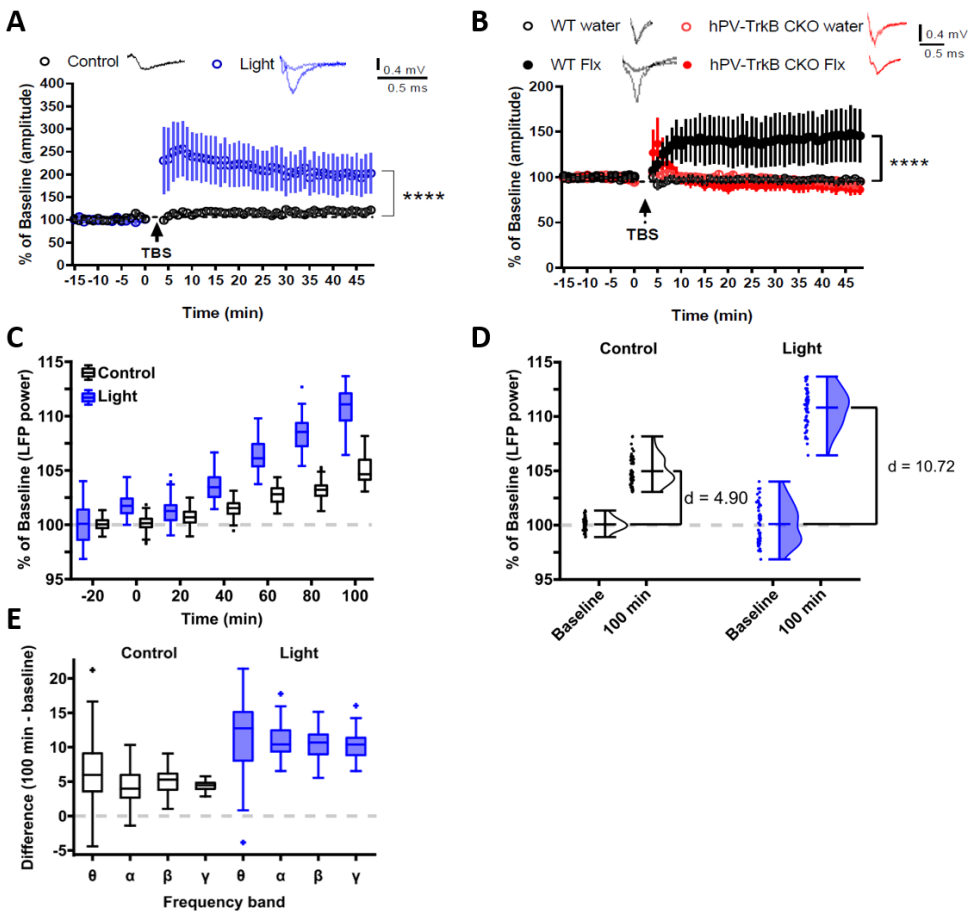

Fig. 2. TrkB in PV cell enhances network activity.

(A) LTP recordings from layer II/III in the V1. Theta-burst stimulation (TBS) results in LTP in slices where optoTrkB has been activated for 30 seconds 30 minutes prior to LTP induction, but not in control slices. Two-way ANOVA ($p < 0.0001$). n = 6-7 recordings/group randomly recorded from 5 animals.

(B) LTP recordings from layer II/III in the V1 in WT and CKO mice after Flx treatment. TBS induces LTP only in WT mice treated with Flx. Two-way ANOVA with Tukey's post-hoc test comparing treatment in WT and treatment in CKO mice (WT water vs. WT Flx, p = < 0.0001; CKO water vs. CKO Flx, p = 0.8871). n = 7-12 recordings/group from 3 animals.

(C) The broadband (4–112 Hz) LFP power (blue: optoTrkB activated at 470 nm, black: control wavelength at 780 nm) averaged over animals (light = 5, control = 4) for each 20 minute recording session as a function of time after light stimulation. LFP power shows a significant increase over time (Regression analysis; Control: y = 0.04 [%/min]*x [min] + 100.25, $R^2 = 0.7573$, $p < 0.0001$; Light: y = 0.09 [%/min]*x [min] + 101.01, $R^2 = 0.8240$, $p < 0.0001$).

(D) Broadband LFP power increase from baseline period (left plot of each half) to 100-minute after blue light (470nm) stimulation (right plot of each half) was approximately twice as strong after optoTrkB activation (blue, difference in medians: d = 10.72) than after stimulation with control wavelength (780nm) (black, difference in medians: d = 4.90). A Welch's t-test confirmed that the LFP power in the 100-minute condition bins after optoTrkB activation is higher than after control stimulation (Welch's t-test, t = 21.60, $p < 0.0001$).

(E) Changes in frequency bands 100 min after light stimulation compared to baseline. Bars represent means ± SEM, **** $p < 0.00001$.

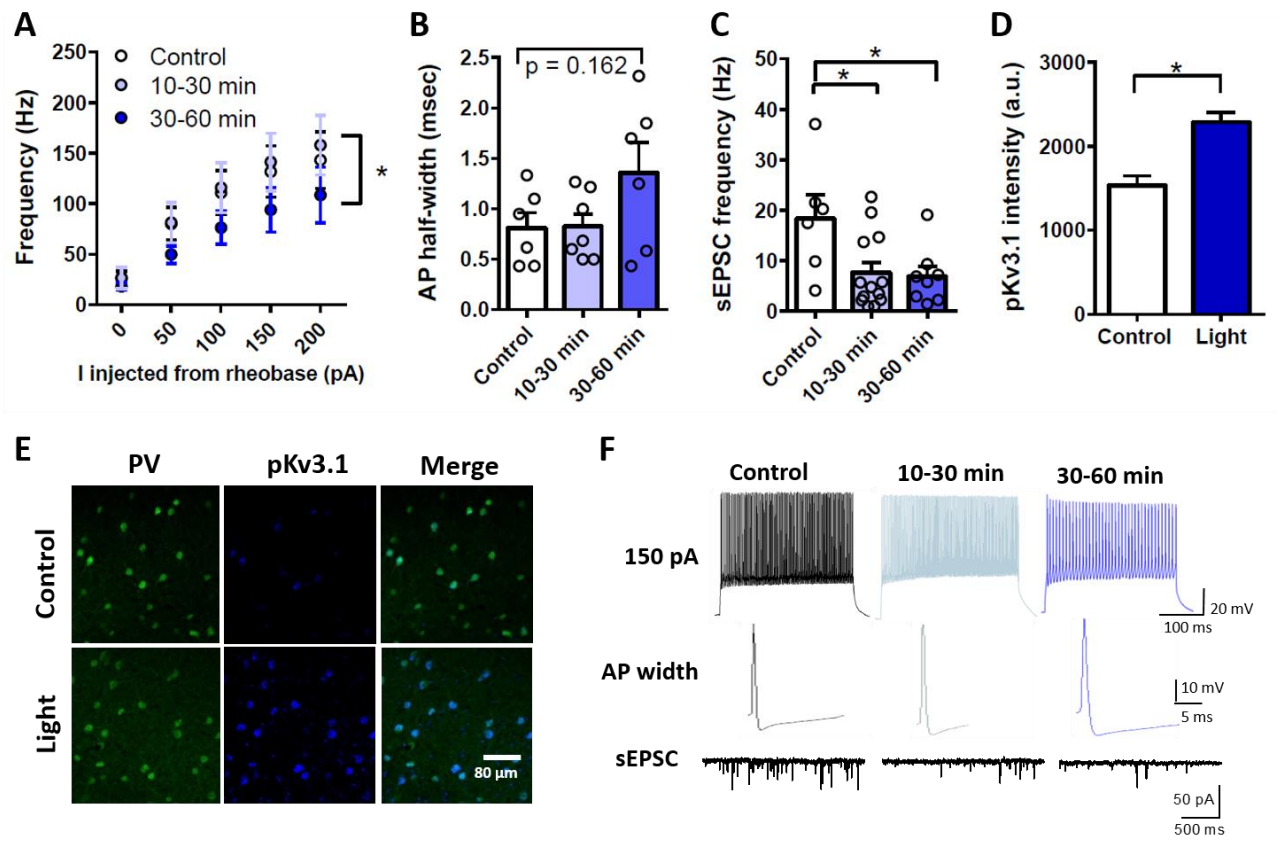

Fig. 3. TrkB activation in PV interneurons reduces cell excitability.
(A) Whole cell patch clamp recordings of intrinsic excitability of optoTrkB-transfected PV cells. Activation of optoTrkB decreases intrinsic excitability of PV cells at 30-60 minutes after light stimulation. Two-way ANOVA with Tukey's post-hoc test comparing control with light stimulation (control vs. 30-60 min, $p = 0.0354$). n = 6-8 recordings/group randomly recorded from 14 animals.
(B) Trends towards larger AP half-width 30-60 min after light stimulation. One-way ANOVA with Bonferroni's post-hoc test (30-60 min, $p = 0.1622$).
(C) sEPSC frequency in PV interneurons is lower at 10-30 minutes after light stimulation as compared to controls. One-way ANOVA with Bonferroni's post-hoc test (10-30 min, $p = 0.0233$; 30-60 min, $p = 0.0261$). n = 6-8 recordings/group randomly recorded from 14 animals.
(D) Light stimulation of optoTrkB results in increased intensity of phospho-Kv3.1 staining in PV interneurons in layer II/III of the V1. Unpaired t-test. n = 6 animals/group; 7 days twice daily light stimulation.
(E) Representative images of PV, phospho-Kv3.1 and merged immunohistochemistry staining.
(F) Representative traces used to estimate intrinsic excitability (top row, 150 pA), AP half-width (middle row) and sEPSC frequency (lower row). AP, action potential; spontaneous excitatory postsynaptic current, sEPSC; Bars represent means ± SEM. * $p < 0.05$; *** $p < 0.0001$; **** $p < 0.00001$

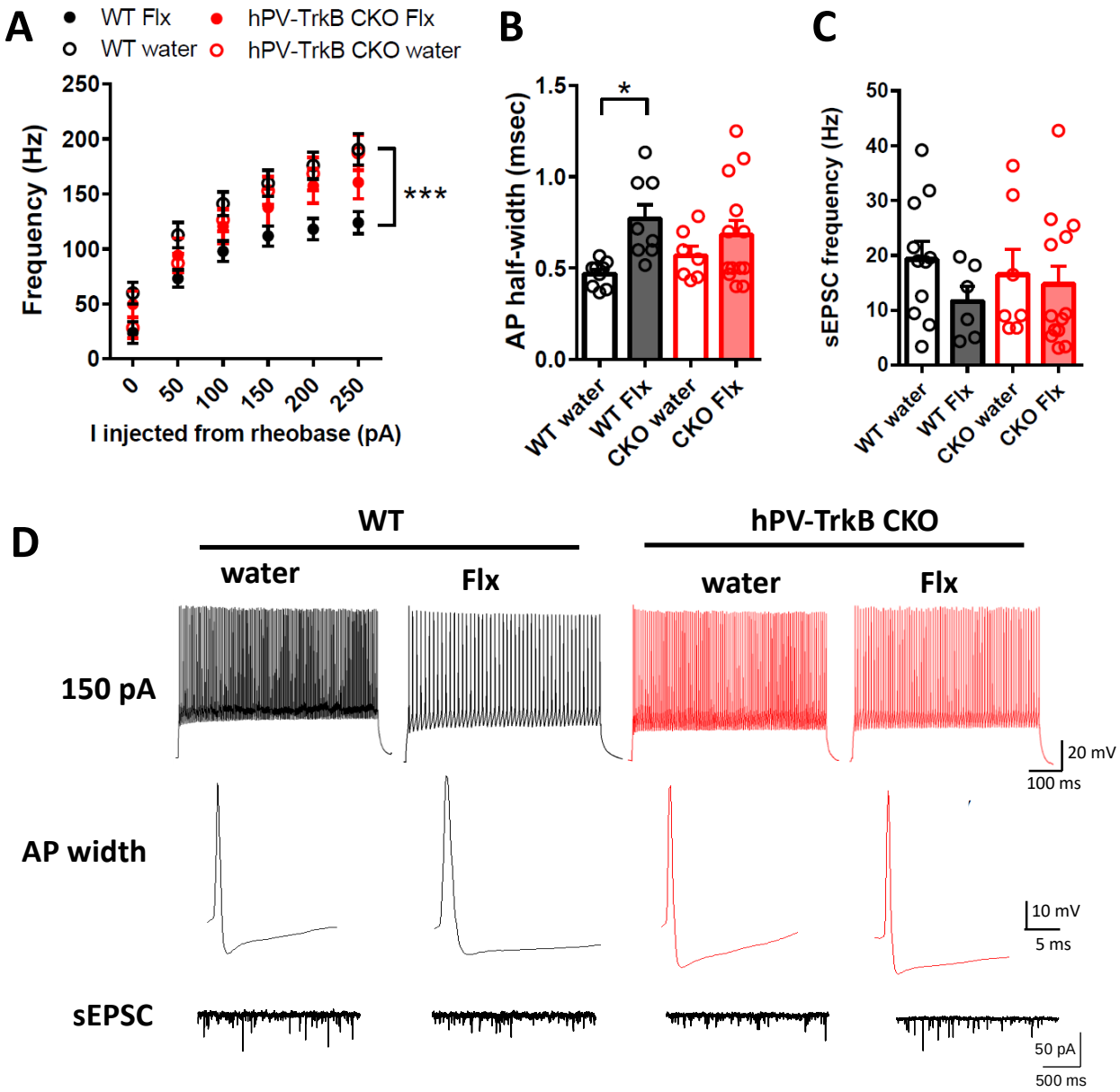

Fig. 4. TrkB expression is necessary for fluoxetine-induced reductions in PV cell excitability.
(A) Whole cell patch clamp analysis of WT and hPV-TrkB CKO mice after chronic Flx treatment. The intrinsic excitability is reduced after Flx treatment in WT mice but not in hPV-TrkB CKO mice. Two-way ANOVA with Tukey's post-hoc test comparing Flx treatment in WT and CKO mice (WT water vs. WT Flx, $p < 0.0001$; CKO water vs. CKO Flx, $p = 0.7068$). n = 7-12 recordings/group from 3 animals.
(B) Flx treatment increases AP half-width in WT mice but not in hPV-TrkB CKO mice. Two-way ANOVA with Tukey's post-hoc test comparing Flx treatment in WT and CKO mice (WT water vs. WT Flx, $p = 0.03$; CKO water vs. CKO Flx, $p = 0.6672$).
(C) Flx treatment induces a trend towards reduced frequency of sEPSC in WT ($p = 0.5397$) but not in hPV-TrkB CKO mice ($p = 0.9866$). Two-way ANOVA with Tukey's post-hoc test.
(D) Representative traces used to estimate intrinsic excitability (150 pA, top row), AP half-width (2nd row) and sEPSC (bottom row) in WT mice treated with water (first column), WT mice treated with Flx (2nd column), CKO mice treated with water (3rd column) and CKO mice treated with Flx (last column). Bars represent means ± SEM. * $p < 0.05$; *** $p < 0.001$; **** $p < 0.0001$

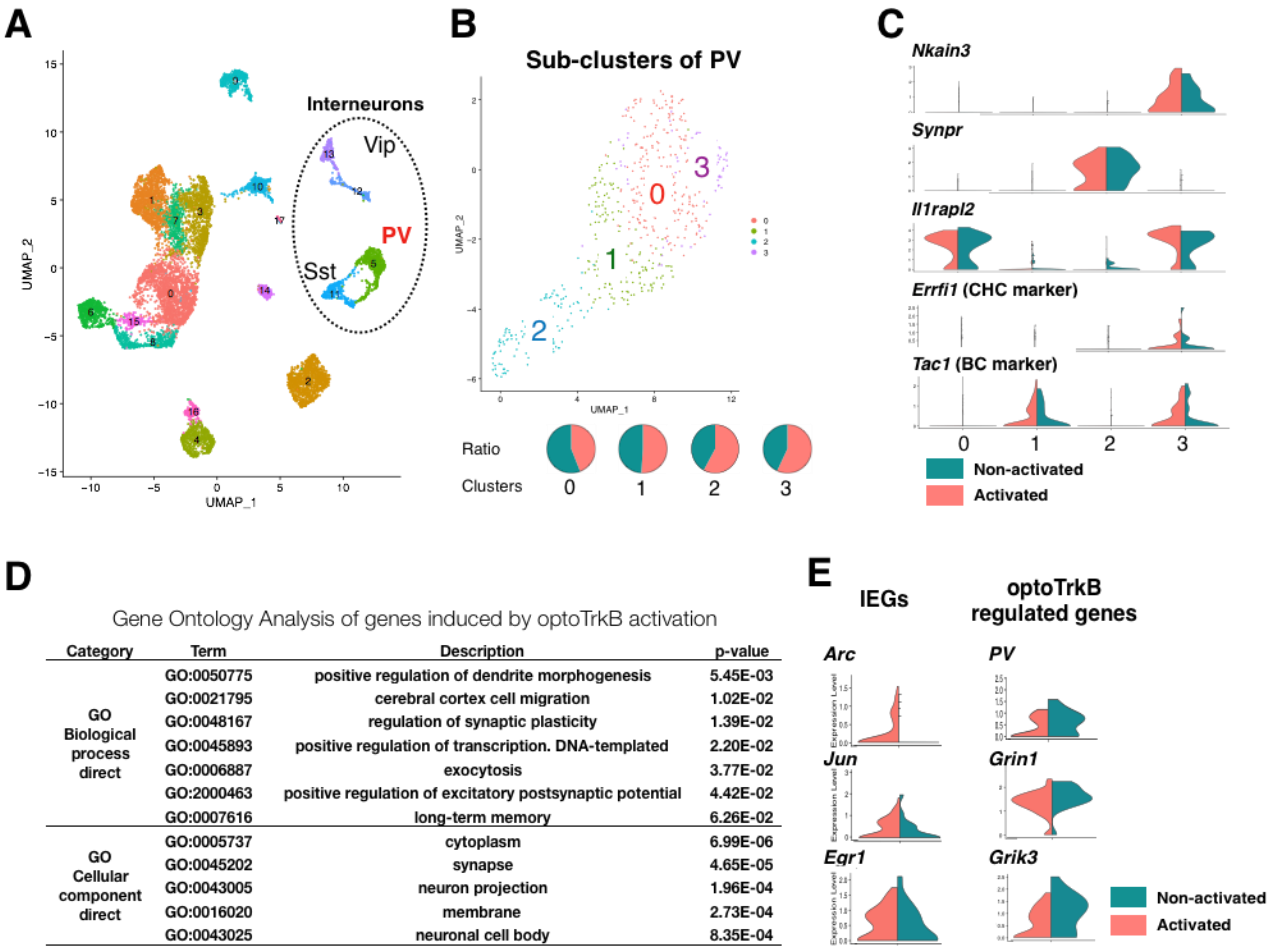

Category	Term	Description	p-value
GO Biological process direct	GO:0050775	positive regulation of dendrite morphogenesis	5.45E-03
	GO:0021795	cerebral cortex cell migration	1.02E-02
	GO:0048167	regulation of synaptic plasticity	1.39E-02
	GO:0045893	positive regulation of transcription. DNA-templated	2.20E-02
	GO:0006887	exocytosis	3.77E-02
	GO:2000463	positive regulation of excitatory postsynaptic potential	4.42E-02
	GO:0007616	long-term memory	6.26E-02
GO Cellular component direct	GO:0005737	cytoplasm	6.99E-06
	GO:0045202	synapse	4.65E-05
	GO:0043005	neuron projection	1.96E-04
	GO:0016020	membrane	2.73E-04
	GO:0043025	neuronal cell body	8.35E-04

Fig. 5. TrkB regulates plasticity-related genes in PV interneurons.
(A) Two-dimensional Uniform Manifold Approximation and Projection (UMAP) plots based on 3,000 differentially expressed (DE) genes for 10,706 cells. After PCA analysis followed by clustering, the cells were grouped into 18 subpopulations including interneurons.
(B) UMAP plots based on 3,000 DE genes for selected 586 cells clustered to PV interneurons. After PCA analysis, the cluster was further divided into 4 groups (PV_0, 1, 2, 3).
(C) Markers differently expressed in each cluster. PV_3 cluster include both Chandelier (CHC) and basket (BS) cells.
(D) Gene ontology (GO) analysis on DE genes between non-light-exposed and light-exposed samples in cluster 3_3.
(E) Selected DE genes of immediate early genes (IEGs) and relevant genes to decreased excitation in cluster PV_3.

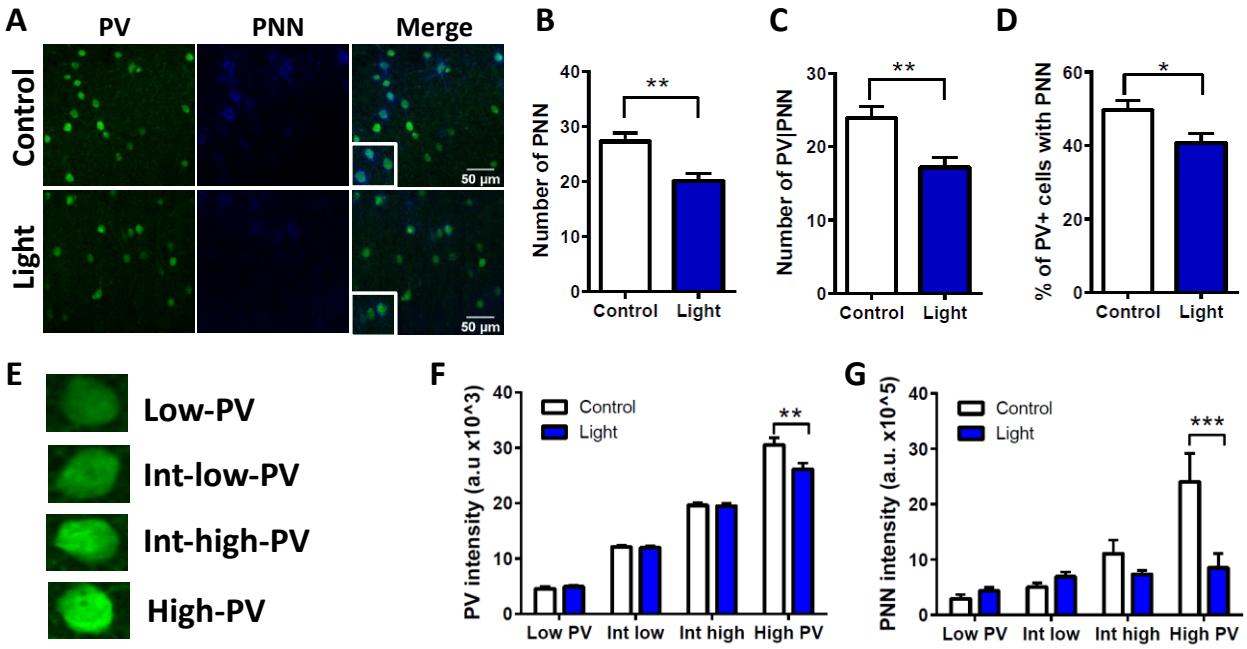

Fig. 6. TrkB activation regulates PV-plasticity.
(A) Representative immunohistochemical images of PV and PNN expression in layer II/III of the V1.
(B-D) Number of cells expressing PV and/or PNN after optoTrkB activation (n = 6 animals/group).
(B) Chronic light stimulation of optoTrkB significantly reduced numbers of PNN positive cells (Unpaired t-test; p 0.0012),
(C) PV/PNN double-positive cells (Unpaired t-test; p = 0.0021), and
(D) PV cells expressing PNN (Unpaired t-test; p = 0.0156).
(E) Representative images of low, intermediate-low, intermediate-high and high PV-expressing cells, where PV interneurons are categorized according to PV intensity.
(F) Image analysis on PV intensities. Chronic stimulation of optoTrkB significantly reduces the PV staining intensities of high PV expressing cells. Two-way ANOVA with Bonferroni's post-hoc test comparing control vs. light stimulated samples (p = 0.0034).
(G) Image analysis on PNN intensities. Activation of optoTrkB decreases PNN intensities in high PV-expressing cells. Two-way ANOVA with Bonferroni's post-hoc test comparing control vs. light stimulated samples (p = 0.0003). Bars represent means ± SEM. * p < 0.05; *** p < 0.0001; **** p < 0.00001

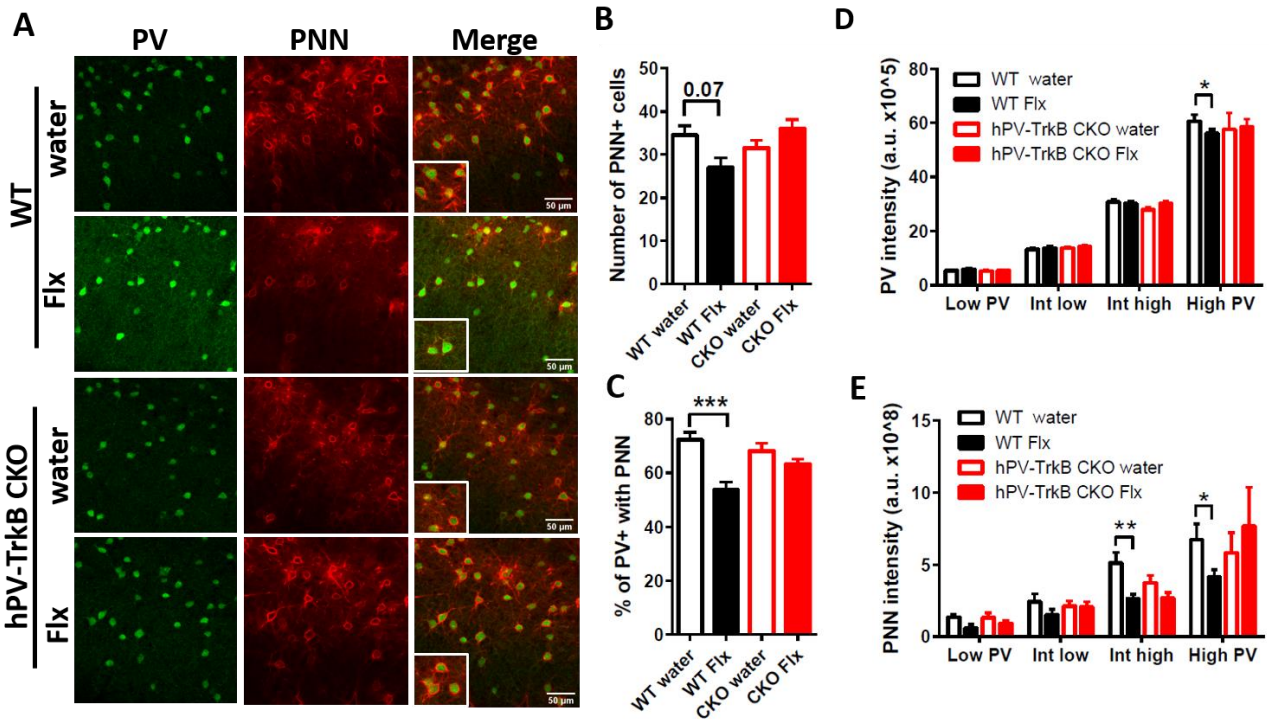

Fig. 7. Fluoxetine-induced PV-plasticity depends on TrkB in PV interneurons.
(A) Representative immunohistochemical images of PV and PNN expression in layer II/III of Flx-treated WT and hPV-TrkB CKO mice. Number (B, C) and intensity (D, E) of cells expressing PV and/or PNN by imaging analysis after Flx treatment.
(B) Flx-treated WT mice show a trend towards lower numbers of PNN ($p = 0.07$).
(C) Flx-treated WT mice have significantly lower percentages of PV interneurons also expressing PNNs, but this effect is abolished in hPV-TrkB CKO mice. Two-way ANOVA with Tukey's post-hoc test comparing Flx treatment in WT and CKO mice (WT water vs. WT Flx, $p = 0.0001$; CKO water vs. CKO Flx, $p = 0.6462$).
(D) Flx treatment decreases PV intensities in high PV expressing cells in WT but this effect is not seen in hPV-TrkB CKO mice. Two-way ANOVA with Tukey's post-hoc test comparing Flx treatment in WT and hPV-TrkB CKO mice (WT water vs. WT Flx, $p = 0.0325$; CKO water vs. CKO Flx, $p = 0.9838$)
(E) Flx treatment reduces PNN intensities in intermediate-high and high PV expressing cells only in WT mice but fails to do so in hPV-TrkB CKO mice. Two-way ANOVA with Tukey's post-hoc test comparing Flx treatment in WT and hPV-TrkB CKO mice (WT water vs. WT Flx, intermediate-high, $p = 0.0014$; high PV, $p = 0.0325$; CKO water vs. CKO Flx, intermediate-high, $p = 0.3217$; high PV, $p = 0.6112$). n = 6-10 animals/group. Bars represent means ± SEM. ** $p < 0.01$; *** $p < 0.001$; **** $p < 0.0001$

493 **STAR Methods**

494 **Lead Contact**

495 Further information and requests for resources and reagents should be directed to and will be

496 fulfilled by the Lead Contact, Juzoh Umemori (Juzoh.umemori@helsinki.fi).

497

498 **EXPERIMENTAL MODEL AND SUBJECT DETAILS**

499 All animal procedures were done according to the guidelines of the National Institutes of Health

500 Guide for the Care and Use of Laboratory Animals and were approved by the experimental Animal

501 Ethical Committee of Southern Finland. Female mice (PV-cre, WT or hPV-TrkB CKO) older than 110

502 days were group housed with *ad libitum* access to food and water. For the shift in ocular dominance

503 paradigm, the mice underwent transparent skull surgery and were monocularly deprived for 7 days.

504

505 **METHOD DETAIL**

506

507 Mice

508 Heterozygous mice with TrkB deletion specifically in PV^{+} interneurons (PV-hTrkB mice; $PV^{pvr/wt}$,

509 $TrkB^{flx/wt}$) were produced by mating females of heterozygous PV specific Cre line ($PV^{pvr/wt}$) (Pvalb-

510 IRES-Cre, JAX: 008069, Jackson laboratory) (Hippenmeyer et al., 2005) and male of homozygous

511 floxed TrkB mice ($TrkB^{flx/flx}$) (Minichiello et al., 1999). Single floxed mice ($TrkB^{flx/wt}$) served as control.

512 For patch-clamp electrophysiology, females of the homozygous PV Cre line ($PV^{pvr/pvr}$) were crossed

513 with males harboring a homozygous TdTomato indicator allele ($Rosa26^{TdT/TdT}$) (Ai14, JAX: 007914,

514 Jackson laboratory)(Madisen et al., 2010) and heterozygous floxed TrkB allele ($TrkB^{flx/wt}$)(Minichiello

515 et al., 1999) to reproduce compound transgenic mice with TrkB deletion and TdT expression

516 specifically in PV interneurons ($PV^{pvr/wt}$, $TrkB^{flx/wt}$, $Rosa26^{TdT/wt}$) (hPV-TrkB CKO) and wild-type allele

517 in TrkB ($PV^{pvr/wt}$, $TrkB^{wt/wt}$, $Rosa26^{TdT/wt}$) (WT). All of the parental strains were back-crossed with
518 C57BL/6J for more than six generations. To assure the complete closure of the critical periods the
519 mice were older than 110 days at the start of the experiments. The mice were kept under 12h
520 light/dark cycle with light on at 6 am and *ad libitum* access to food and water.
521

522 Construction of optoTrkB

523 Photolyase homology region (PHR) domain of optoTrkB (Chang et al., 2014) was optimized in codon
524 usage for mice and connected with a flexible tag (Kennedy et al., 2010) to the C-terminus of a full-
525 length mouse TRKB, as previously described (Umemori et al, submitted). For cre-dependent
526 expression of optoTrkB, a double floxed inverted open-reading frame (DIO) structure (Fenno et al.,
527 2014) of optoTrkB (DIO-optoTrkB) was constructed (Figure S1A). We artificially synthesized DNA
528 including human Synapsin promoter (Kügler et al., 2001), lox2272 (Lee & Saito, 1998), loxP, inverted
529 optoTrkB sequence [PHR, flexible tag (Kennedy et al., 2010), mouse full-length TrkB
530 (NM_001025074)], lox2272, loxP, and cloned into pFCK(0.4)GW (a gift from Pavel Osten) (Addgene
531 plasmid # 27229 ; http://n2t.net/addgene:27229; RRID:Addgene_27229) (Dittgen et al., 2004) using
532 PacI and EcoRI cloning sites (Figure S1a). Furthermore, for electrophysiological studies, we
533 constructed DIO-optoTrkB expressing TdTomato (Shaner et al., 2004) (DIO-optoTrkB-IRES-TdT)
534 (Figure S1C). A fragment of Internal ribosome entry site (IRES) with TdTomato was amplified by PCR
535 with primers (5'- ggcgcgCCCCCCTCTCCCTCCCCCCC -3' and 5'-
536 ggcgcgccTTACTTGTACAGCTCGTCCATGCCGTACAG -3') using Hot start Q5® polymerase (NEB, USA)
537 from LeGO-iT (a gift from Boris Fehse) (Addgene plasmid # 27361 ; http://n2t.net/addgene:27361 ;
538 RRID:Addgene_27361) (Weber et al., 2010), and cloned into pCR ™ Blunt II-TOPO® vector
539 (ThermoFisher Scientific). Then the sequence was confirmed by sequencing and sub-cloning into

540 AscI cloing sites of DIO-optoTrkB (Figure S1A) to construct DIO-optoTrkB-IRES-TdT. Cre-dependent
541 Inversions of DIO-optoTrkB and DIO-optoTrkB-IRES-TdT were confirmed in HEK293 cells co-
542 transfected with the DIO-vectors and plasmids expressing Cre recombinase followed by PCR (Set1
543 (Figure S1B), and immunocytology (Figure S1D). The following primers were used to confirm the
544 inversion of DIO-optoTrkB:
545 Set1 (5'- AGTCGTGTCGTGCCTGAGA -3' and 5'- GAAATTTATGTGCCGCAGGT -3'); Set2 (5'-
546 CTGCTGGCAAAGGCTATTTC -3' and 5'- GGGCCACAACTCCTCATAAA -3').
547

548 Virus generation

549 DIO-optoTrkB/DIO-optoTrkB-IRES-TdT, pLP1, pLP2, and pVSVG were co-transfected into HEL293FT
550 cells by jetPEI® (Polyplus Transfection®) according to the manufacturer's instruction, for producing
551 lentivirus through a previously reported method (Hioki et al., 2007). Briefly, 3µg of the plasmids was
552 transfected into HEL293FT cells and cultured on a poly-D-Lysine coated dish containing pre-warmed
553 Opti-MEM®I medium (2% FBS) for 72 hrs. Then the culture supernatant was collected and
554 exchanged with a new Opti-MEM®I medium (2% FBS) followed by incubation for 72 hrs. The culture
555 supernatant was collected again and centrifuged at 4 °C at 2000 g for 10 min. The supernatant was
556 then concentrated with Amicon® Centrifugal Filter Units Ultra -15 (Millipore®) into less than 10ml.
557 The concentrated solution was purified using the sucrose gradient method (Tiscornia et al., 2006)
558 and aliquots were stored at -80 °C until use. From one aliquot the p24 capsid protein concentration
559 was measured to estimate the infection unit (IU).
560

561 Virus injection

562 PV-cre mice were anaesthetized with 2.5% isoflurane and DIO-optoTrkB (p24 concentration/titer
563 4,04 x 10^7) was stereotaxically injected into the binocular area of the V1, previously identified

564 through optical imaging (see below) and using blood vessels as landmarks. DIO-optoTrkB was
565 stimulated with blue LED light (470nm) through the transparent skull during monocular deprivation
566 twice a day for 30 seconds at 8-10 am and 4-6 pm. Blue LED light was provided by a BLS Super High
567 Power Fiber-Coupled LED Light Sources (BLS-FCS-0470-100, Mightex) connected to a BioLED Light
568 Source Control Modules (BLS-3000-2, Mightex). To avoid light exposure through the skull, the
569 transparent skull was covered by black nail polish between light stimulation sessions.ht
570

571 ## Surgery

572 For chronic imaging of intrinsic signals, the animals underwent transparent skull surgery as
573 described previously (Steinzeig et al., 2017).
574

575 ## Fluoxetine treatment

576 Fluoxetine (Bosche Scientific, NJ, USA) was administered via drinking water (0.08 mg/ml),
577 corresponding to a dose of approximately 8-12 mg/kg/day, and kept in light-protected bottles. The
578 drinking water of both the control and fluoxetine group contained 0.1 % saccharin, was changed
579 twice a week and the consumption was monitored. Drug treatment started after transparent skull
580 surgery and continued throughout the whole experiment.
581

582 ## Monocular deprivation and virus stimulation

583 The animals were anaesthetized with intraperitoneal injection as described above. The eye lashes
584 were trimmed and the eye lid margins were sutured shut with 3 mattress sutures. To prevent
585 postoperative infections, an eye ointment containing dexamethasone was applied. The eyes were
586 checked daily until reopening, re-sutured if needed, and mice with signs of corneal injury were

587 excluded from the experiments.

588

589 ## Optical imaging of intrinsic signals

590 We determined the strength of neuronal responses to stimulation of either eye in the binocular
591 region of the V1 using imaging of intrinsic signals (IOS) (Kalatsky & Stryker, 2003) before (IOS I; IOS
592 III) and after (IOS II; IOS IV) monocular deprivation. The animals were chamber anaesthetized with
593 1.8% isoflurane in a 1:2 mixture of O_2/air and then intubated and ventilated with 1.2% isoflurane in
594 the same mixture.

595 Intrinsic optical signal responses were recorded from the V1 of the right hemisphere according to a
596 previously described protocol (Kalatsky & Stryker, 2003), which was modified for the measurement
597 of OD plasticity (Cang et al., 2005).

598

599 ## Data analysis of optical imaging

600 Cortical maps were computed based on the acquired frames using Fourier decomposition to extract
601 the signal from biological noise using an analysis software package for continuous recording of
602 optical intrinsic signals (VK Imaging, USA) (Kalatsky & Stryker, 2003). The ODI was then calculated
603 for every pixel within the binocularly responding region based on the formula (C-I)/(C+I), where "C"
604 refers to the response magnitude of the contralateral eye and "I" to that of the ipsilateral eye. For
605 each animal, several ODIs were collected and then averaged. Positive ODI values represent
606 contralateral dominance, negative represent ipsilateral dominance, while ODI values of 0
607 correspond to equally strong contralateral and ipsilateral eyes.

608

609 In vivo electrophysiology

610 To measure oscillations in the binocular region of the optoTrkB transfected area, PV-cre mice
611 underwent transparent skull surgery and optoTrkB was injected as described above. Under 15%
612 urethane anesthesia (in PBS), a hole for a 16 channel optrode (A1x16-10mm-100-177-OA16LP,
613 NeuroNexus, Ann Arbor, MI, USA) was drilled next to the injection site and a hole for a ground
614 electrode next to lambda. The animals were head-fixed and the optrode was covered with DiI and
615 slowly inserted into the V1 to a depth of about 2200 µm. The data was recorded using a Smartbox
616 (NeuroNexus, Ann Arbor, MI, USA) at a sampling rate of 20 kHz. After collecting a 20 minute baseline,
617 optoTrkB was stimulated for 30 seconds with blue LED light and recorded for 2h, separated into 20-
618 minute blocks. Finally, the animals were transcardially perfused and the brains fixed with 4% PFA. To
619 confirm the position of the electrodes and co-localization with optoTrkB, 250 µm coronal slices were
620 cut on a vibratome.

621 The digitized data were first offline notch filtered at 50 Hz by the Python RHD2000 interface provided
622 by Intan. Afterwards, the data were band-pass filtered between 4 and 150 Hz, using a 2nd order
623 Butterworth filter with zero-phase shift, and then downsampled to a sampling rate of 1 kHz to
624 extract the local field potential (LFP) component. The LFP for each electrode contact was normalized
625 to zero and the underlying current source density (CSD) was calculated as the second spatial
626 derivative, using previously published methods (Voigt & Kral, 2019).

627 Time-frequency analysis of the CSD data was performed by wavelet filtering using 36 Morlet
628 wavelets with a width parameter m = 6 and with frequencies ranging from 4 to 112 Hz with log-
629 constant scaling. For further analyses, the signal from all electrodes that were identified to reside in
630 areas with optoTrkB expression by the histological analysis was averaged, and the data were binned
631 into non-overlapping 20 seconds bins. Morlet power spectra were estimated by computing the
632 averaged magnitude over all bins of the 20-minute recording period per condition. For statistical

633 analysis, broadband power in the 20-minute baseline period and the 20-minute period beginning
634 100 minutes after LED onset was compared using permutation testing. Surrogate data was generated
635 by 1000 random permutations of condition labels and the effect size was measured using Cohen's
636 d. All data analyses and statistics were performed in Python (ver. 2.7) using SciPy (ver. 0.19.0), the
637 NeuroDSP toolbox (ver. 2.0.1-dev)(Cole et al., 2019), and custom written scripts.
638

639 Electrophysiology in acute slices

640 The brains of optoTrkB-infected PV-cre mice were dissected in darkness using red light illumination,
641 and kept in the dark throughout the whole experiment. The brains, including brains of fluoxetine-
642 treated WT and hPV-TrkB cKO mice, were dissected and immersed in ice-cold dissection solution
643 containing (in mM): 124 NaCl, 3 KCl, 1.25 NaH_2PO4, 1 $MgSO_4$, 26 $NaHCO_3$, 15 D-glucose, 9 $MgSO_4$
644 and 0.5 $CaCl_2$. The cerebellum and anterior part of the brain were removed and coronal 350µm brain
645 slices of the V1 were cut on a vibratome (Leica Biosystems). Slices were divided into two groups and
646 allowed to recover for 30 min at 31-32°C in artificial cerebrospinal fluid (ACSF) containing (in mM):
647 124 NaCl, 3 KCl, 1.25 NaH_2PO_4, 1 $MgSO_4$, 26 $NaHCO_3$, 15 D-glucose, and 2 $CaCl_2$ and bubbled with 5%
648 CO_2/95% O_2.
649 OptoTrkB-transfected slices in one of the groups were acutely stimulated for 30 seconds with blue
650 light after transferring them to the recording chamber, whereas the transfected slices in the other
651 group were kept in darkness.
652 Field excitatory postsynaptic currents (fEPSPs) were recorded in an interface chamber (32°C) with
653 ACSF-filled glass microelectrodes (2-4 MΩ) positioned within layer II/III of the V1 using an Axopatch
654 200B amplifier (Molecular devices, San Jose, CA, USA). Electric stimulation (100 µsec duration) was
655 delivered with a bipolar stimulation electrode placed at the border of the white matter (WM) and
656 layer VI. Baseline synaptic responses were evoked every 20 seconds with a stimulation intensity that

657 yielded a half-maximum response. After obtaining a 15 minute stable baseline, θ burst stimulation
658 (TBS) (4 sweeps at 0.1 Hz, each sweep with 10 trains of 4 pulses at 100 Hz at 200 ms intervals) was
659 delivered and field potentials in response to 0.05 Hz stimulation were recorded for additional 45
660 minute. WinLTP (0.95b or 0.96, www.winltp.com) was used for data acquisition and analysis.
661
662 To measure intrinsic excitability, the brains of PV-cre mice transfected with the DIO-optoTrkB-IRES-
663 TdT lentivirus were dissected as described above but cut in a protective NMDG ACSF (Ting et al.,
664 2014) containing (in mM): 92 NMDG, 2.5 KCl, 1.25 NaH_2PO_4, 30 $NaHCO_3$, 20 HEPES, 25 glucose, 2
665 thiourea, 5 Na-ascorbate, 3 Na-pyruvate, 0.5 $CaCl_2 \cdot 4H_2O$ and 10 $MgSO_4 \cdot 7H_2O$, pH 7.3–7.4 The slices
666 were allowed to recover at 32°C for 10 min, after which they were transferred to modified ACSF
667 containing (mM): 92 NaCl, 2.5 KCl, 1.25 NaH_2PO_4, 30 $NaHCO_3$, 20 HEPES, 25 glucose, 2 thiourea, 5
668 Na-ascorbate, 3 Na-pyruvate, 2 $CaCl_2 \cdot 4H_2O$ and 2 $MgSO_4 \cdot 7H_2O$, pH 7.3-7.4 for storage. Recordings
669 were done in submerged chamber perfused with normal ACSF (32°C).
670 Whole cell patch clamp recordings from the TdT expressing PV cells were obtained under visual
671 guidance under ambient light with glass microelectrodes (3-5 MΩ) filled with a low Cl^--filling solution
672 containing (in mM): 135 K-gluconate, 10 HEPES, 2 KCl, 2, $Ca(OH)_2$, 5 EGTA, 4 Mg-ATP, 0.5 Na-GTP
673 using a Multiclamp 700A amplifier (Axon Instruments, USA). Uncompensated series resistance (Rs)
674 was monitored by measuring the peak amplitude of the current response to a 5 mV step. Only
675 experiments where Rs < 30 MΩ, and with < 20 % change in Rs during the experiment, were included
676 in analysis.
677 Intrinsic excitability was measured in current clamp mode by injecting currents ranging from -50 to
678 600 pA for 600 ms in 50 pA steps from the resting membrane potential of -60/-70 mV. The recordings
679 were analyzed in Clampfit (Molecular Devices, San Jose, CA, USA) programs. A minimum of three
680 action potentials (AP) were averaged based on their AP half-width (10th AP at 200pA injected from

681 rheobase). sEPSCs were recorded under voltage clamp at -70 mV and analyzed in Clampfit
682 (Molecular Devices, San Jose, CA, USA). The threshold for detection of inward sEPSC events was
683 three times the baseline noise level, and all detected events were verified visually.
684

685 ## Sample collection

686 For collecting tissue samples for qPCR and Western Blot experiments, the brains of optoTrkB infected
687 PV-cre mice were dissected and immersed in ice-cold dissection solution containing (in mM): 124
688 NaCl, 3 KCl, 1.25 NaH_2PO_4, 1 $MgSO_4$, 26 $NaHCO_3$, 15 D-glucose, 9 $MgSO_4$ and 0.5 $CaCl_2$. The V1 was
689 dissected and incubated at 31-32°C in artificial cerebrospinal fluid (ACSF) containing (in mM): 124
690 NaCl, 3 KCl, 1.25 NaH_2PO_4, 1 $MgSO_4$, 26 $NaHCO_3$, 15 D-glucose, and 2 $CaCl_2$ and bubbled with 5%
691 CO_2/95% O_2. The tissue samples were either immediately collected in NP lysis buffer and
692 homogenized (control), or stimulated with blue LED light for 30 seconds and collected and
693 homogenized after 15 minutes, 30 minutes or 60 minutes. All of the procedures were done in dark
694 conditions. The samples were further used for qPCR and Western Blot analysis.
695

696 ## Western Blot

697 The samples were centrifuged (16000 g, 15 min at +4°C) and the supernatant was used to measure
698 the protein concentrations using the Lowry method (Biorad DC protein assay; Lowry et al, 1951). The
699 samples were separated in a SDS-PAGE (2-4% gradient gel, NuPage™; Invitrogen, CA, USA) and
700 blotted to a PVDF membrane (300 mA, 1 h, + 41°C). The membranes were washed in Tris Buffer
701 Solution with 0,001% Tween ®20 (TBST), blocked in TBST with 3% BSA for 1 hour at room
702 temperature and incubated in primary antibody solutions (in TBST with 3% BSA) directed against:
703 phosphorylated and non-phosphorylated forms of TrkB (Y816, Y705/6, Y515) and CREB at +4°C for

704 overnight. After washing in TBST, the membranes were further incubated in secondary antibody
705 solutions (TBST with 5% Non-Fat Dry Skinned Milk and Horseradish Peroxidase conjugated secondary
706 antibodies Goat Anti-Rabbit/Mouse, 1:10000) for 2 hours at room temperature. After washing with
707 TBST and rinsing with PBS, secondary antibodies were visualized by an electrochemiluminescence
708 kit (ECL plus, Thermo Scientific®, CA, USA) according to the manufactures instruction, and detected
709 using a FUJIFILM LAS-3000 dark box.
710

711 ## qPCR

712 RNA was purified from the lysate following the manufacturer's protocol using a combined protocol
713 of QIAzol® (Qiagen) and NucleoSpin® (Macherey-Nagel). Briefly, the aqua layer was isolated after
714 Qiazol and chloroform extraction. The RNA was washed in 100% ethanol and the DNA was digested
715 in the spin columns. The purified RNA was then reverse transcribed to cDNA using Maxima First
716 Strand cDNA Synthesis Kit (Thermo-Scientific). The amount of cDNA synthesized from the target
717 mRNA was quantified by real-time PCR (qPCR). The following primers were used to amplify specific
718 cDNA regions of the transcripts of interest:
719 PV (5'-TGTCGATGACAGACGTGCTC-3' and 5'-TTCTTCAACCCCAATCTTGC-3').
720

721 ## Immunohistochemistry

722 Animals were transcardially perfused with PBS followed by chilled 4% paraformaldehyde (PFA) in
723 PBS. Brains were removed under ambient light and left for fixation in 4% PFA overnight at +4 °C. For
724 cutting, the brains were embedded in 3% agar and cut into 40 µm coronal visual cortical sections
725 using a vibratome (Leica Biosystems). After washing with PBST (1x PBS and 0.2% TritonX100), the
726 sections were incubated in 10% donkey serum (Vector Laboratories, UK) and 3% Bovine Serum

727 Albumin (BSA) (Sigma-Aldrich) in PBST for 30 minutes at room temperature. Next, the sections were
728 incubated with the following antibodies: 1) guinea pig anti-parvalbumin (1:1000; Synaptic Systems,
729 Göttingen, Germany), 2) biotinylated lectin from Wisteria floribunda (WFA; 1:200; Sigma-Aldrich,
730 Helsinki, Finland), and 3) rabbit anti-phospho Kv3.1 (1:100; Phosphosolutions, Colorado, USA)
731 overnight at +4° C. After washing in PBST, the samples were further incubated in: 1) goat anti-guinea
732 pig secondary antibody conjugated with Alexa Fluor647/546 (1:1000; Abcam, Cambridge, UK/Life
733 technologies, Carlsbad, California, USA), 2) streptavidin conjugated with Alexa Fluor488 (1:1000;
734 Thermofisher, Waltham, Massachusetts, USA), or 3) Goat anti-rabbit conjugated with Alexa Fluor
735 647 (1:1000; Life technologies, Carlsbad, California, USA) for 2 hours at room temperature protected
736 from light. After final washing in PBS, the sections were transferred to 0.1M PB with gelatin,
737 mounted on glass slides and covered with DAKO mounting medium (Sigma Aldrich, Helsinki,
738 Finland).
739

740 Image acquisition and analysis

741 Quantitative analysis of immunostainings was performed blind. Images were taken from the V1
742 according to the mouse brain atlas.
743 Laser scanning confocal microscopy was used to detect PV positive (PV^+), PNN positive (PNN^+),
744 double positive (PV^+PNN^+) and pKv3.1-positive cells. Images were obtained using a confocal
745 microscope LSM 700 (Carl Zeiss) equipped with a 10× objective lens (10x Plan-Apochromat 10x/0.45,
746 Carl Zeiss) and imaging Software ZEN 2012 lite (Zeiss, Vantaa, Finland). From each section, a z-stack
747 containing at least 10 consecutive images was obtained. A minimum number of 3 sections per
748 animal were imaged using the same microscope and the same camera settings for all samples. Image
749 processing was done using ImageJ software version 1 (National Institutes of Health). All images in
750 each z-stack were analyzed and the number of cells was averaged per z-stack.

751 To determine the PV cell populations, frequency distribution analyses were performed on PV
752 intensities taken from non-stimulated optoTrkB samples or control WT samples to serve as reference
753 group. The PV cell populations were defined as low PV (0-8000 a.u.), intermediate-low PV (int-low
754 PV, 8000-16000 a.u.), intermediate-high PV (int-high, 16000-24000 a.u.) and high PV (24000-36000
755 a.u.) expressing cells and these criteria were applied to the light stimulated samples.

756

757 Nuclei preparation

758 Single nuclei RNA sequencing (snRNA-seq) was conducted by following previously reported methods
759 with some modifications (Bakken et al., 2018; Krishnaswami et al., 2016) (Figure S3A). Considering
760 that optoTrkB is sensitive to light stimulation, we used snRNA-seq instead of single cell RNA
761 sequencing (scRNA-seq) after FACS selected by TdTomato fluorescence, to avoid laser-induced
762 optoTrkB activation during FACS. There is a good correlation of gene expression and gene detection
763 sensitivity in each cell between SnRNA-seq and scRNA-seq (Bakken et al., 2018), and snRNA-seq has
764 several advantages, such as reduced dissociation bias and dissociation-induced transcriptional stress
765 responses (Wu et al., 2019). Tissue samples were obtained bilaterally from the visual cortex of adult
766 female PV-cre mice infected with DIO-optoTrkB-TdT. After deep anesthesia with pentobarbital, the
767 mice were perfused with ice-cold NMDG ACSF (Ting et al., 2014) consisted of 0.5 mM $CaCl_2$, 25mM
768 D-Glucose, 98 mM HCl, 20 mM HEPES, 10 mM $MgSO_4$, 1.25 mM NaH2PO4, 3 mM Myo-inositol, 12
769 mM N-acetylcysteine, 96 mM N-methyl-D-glucamine, 2.5 mM KCl, 25 mM $NaHCO_3$, 5 mM sodium L-
770 Ascorbate, 3 mM sodium pyruvate, 0.01 mM Taurine, and 2 mM Thiourea, bubbled with a carbogen
771 gas (95% O_2 and 5% CO_2), and the brains were isolated and sliced on a vibratome (MICROM, HM
772 650V, Thermo Fisher Scientific) in NMDG ACSF (Ting et al., 2014). Then, the slices were exposed to
773 blue LED light (30 seconds), and incubated in a modified HEPES ACSF including 92 mM NaCl, 2.5 mM
774 KCl, 1.25 mM NaH_2PO_4, 30 mM $NaHCO_3$, 20 mM HEPES, 25 mM glucose, 2 mM thiourea, 5 mM Na-

775 ascorbate, 3 mM Na-pyruvate, 2 mM $CaCl_2$, 2 mM $MgSO_4$, 3 mM Myo-inositol, and 0.01 mM Taurine
776 for one hour. The visual cortex was bilaterally isolated from the slices under a microscope using red
777 light illumination, and tissues were transferred to pre-cooled Dounce homogenizers filled with cold
778 homogenization buffer (250 mM sucrose, 25 mM KCl, 5 mM MgCl2, 10 mM Tris buffer, pH 8.0, 1 µM
779 DTT, 1× protease inhibitor (cOmplete, Sigma-aldrich), 0.4 U/µl RNase Inhibitor (Promega), 0.2 U/µl
780 Superasin (Thermo Fisher Scientific), 0.1% (v/v) Triton X-100 (Sigma-Aldrich), 10 µg/ml
781 Cyclohexamide (Sigma-Aldrich), 10 µg/ml Actinomycin D (Sigma-Aldrich), 10 ng/ml Hoechst 33342
782 (Thermo Fisher Scientific)). The tissues were homogenized with five strokes of the loose pestle,
783 followed by 10 strokes of the tight pestle. Finally, nuclei of the tissues were obtained by filtration
784 through a BD Falcon tube with a cell strainer cap (BD). All procedures were performed with RNase
785 free in the dark condition.
786

787 Immunostaining and sorting of nuclei

788 The nuclei were centrifuged (1,000 x g, 8 min, 4 °C) and resuspended in staining buffer (PBS, pH 7.4,
789 with 0.5% RNase-free BSA (Promega) and 0.2 U/µl of RNasin Plus RNase inhibitor (Promega)).
790 Samples were incubated in blocking/washing buffer (PBS with 0.5% BSA). The nuclei were incubated
791 with mouse monoclonal anti-NeuN antibody (Sigma-Aldrich, MAB377, 1:5000) or purified mouse
792 IgG1k (BD Pharmigen, 554121, 1:5000) as a negative control for staining and sorting for 30 min with
793 rotation at 4 °C. Then the samples were washed in staining buffer by inverting the tubes several
794 times, and were centrifuged for 5 min at 400g at 4 °C. The pellet nuclei were re-suspended in 500 µl
795 of staining buffer containing goat anti-mouse Alexa Fluor 488 secondary antibody (Fisher Scientific)
796 with a final dilution of 1:5000, and were incubated with rotation for 30 min at 4 °C followed by
797 washing with blocking/washing buffer.
798

799 FACS of nuclei

800 Hoechst 33342 and NeuN positive nuclei stained with Alexa488 were sorted and collected by BD
801 Influx cell sorter (BD Biosciences) (Figure S3B). After checking the quality, collected nuclei were
802 loaded on Chromium Controller (10x Genomics).

803

804 Single nuclei RNA sequencing (snRNA-seq)

805 Preparation of cDNA Library was done using Chromium Single Cell 3' Gene Expression v3 library
806 preparation kit (10x Genomics), and sequenced with NovaSeq 6000 (Illumina) with read lengths:
807 28bp (Read 1), 8bp (i7 Index), 0 bp (i5 Index) and 89bp (Read 2). Data was pre-processed using
808 CellRanger 3.0. The reads are mapped to reference genome that included introns, and we obtained
809 3,789 and 6,923 cells with approximately 10k median reads per cell (Figure S4).

810

811 Data analysis for snRNA-seq

812 Data analysis was carried out using Chipster version 3.16 (Kallio et al., 2011), which utilizes Seurat
813 v3 (Butler et al., 2018). Cells with more than 7,000 and less than 100 reads were filtered out, and
814 reads for the remaining cells were scaled logarithmically. Based on results for plotting variance
815 against expression, 3000 most highly varied genes in 10,706 cells were used for clustering and
816 sample integration. By Seurat's integrated analysis (Butler et al., 2018), 20 canonical components
817 were used for finding anchors and 20 principal components to integrate the samples together.
818 Clusters were obtained using UMAP(Mcinnes et al., 2018) with 20 principal components and
819 resolution 0.5 (Figure S5A, and S5B). This resulted in 18 clusters and we identified the clusters of
820 pyramidal and interneurons, using *Gad1* and *Slc6a1*, and further *Parvalbumi*n (*Pvalb*)- , *Paired box*
821 *protein* (*Pax6*)-, *Vasoactive intestinal peptide* (*VIP*)-, and *Somatostatin* (*Sst*) previously reported
822 markers (Tasic et al., 2018)(Fig. 5A) (Figure S5C). Then a subset of data containing only parvalbumin-

823 positive interneurons was selected and clustered again by UMAP with the same parameters resulting
824 in four different clusters (Fig. 5B) (Figure S6A and S6B). Markers and differentially expressed genes
825 between non- and light- exposed samples were detected in each cluster (Figure S6D) (Table S3-6).
826 Pathway and gene ontology analysis was carried out with DAVID (Huang et al., 2009).
827

828 ## Statistical analysis

829 All statistical graphs were generated using Graphpad Prism v.6.07. Unpaired t-Test, Two-way and
830 one-way ANOVA followed by Tukey's or Bonferroni post hoc tests were also performed using
831 Graphpad Prism v.6.07. The confidence level was set to 0.05 (P value) and all results were presented
832 as means ± s.e.m. All the individual data points are shown in the histograms. The data distribution
833 was assumed to be normal but this was not formally tested. The sample size was determined based
834 on our previous experience.
835

836 ## DATA AND SOFTWARE AVAILABILITY

837 snRNA-seq data is available in the Gene Expression Omnibus, GEO: GSE142797 (after accepting the
838 manuscript). All data are available upon request to the Lead Contact.
839
840
841
842
843
844
845
846
847
848
849
850
851
852
853

Supplemental Information

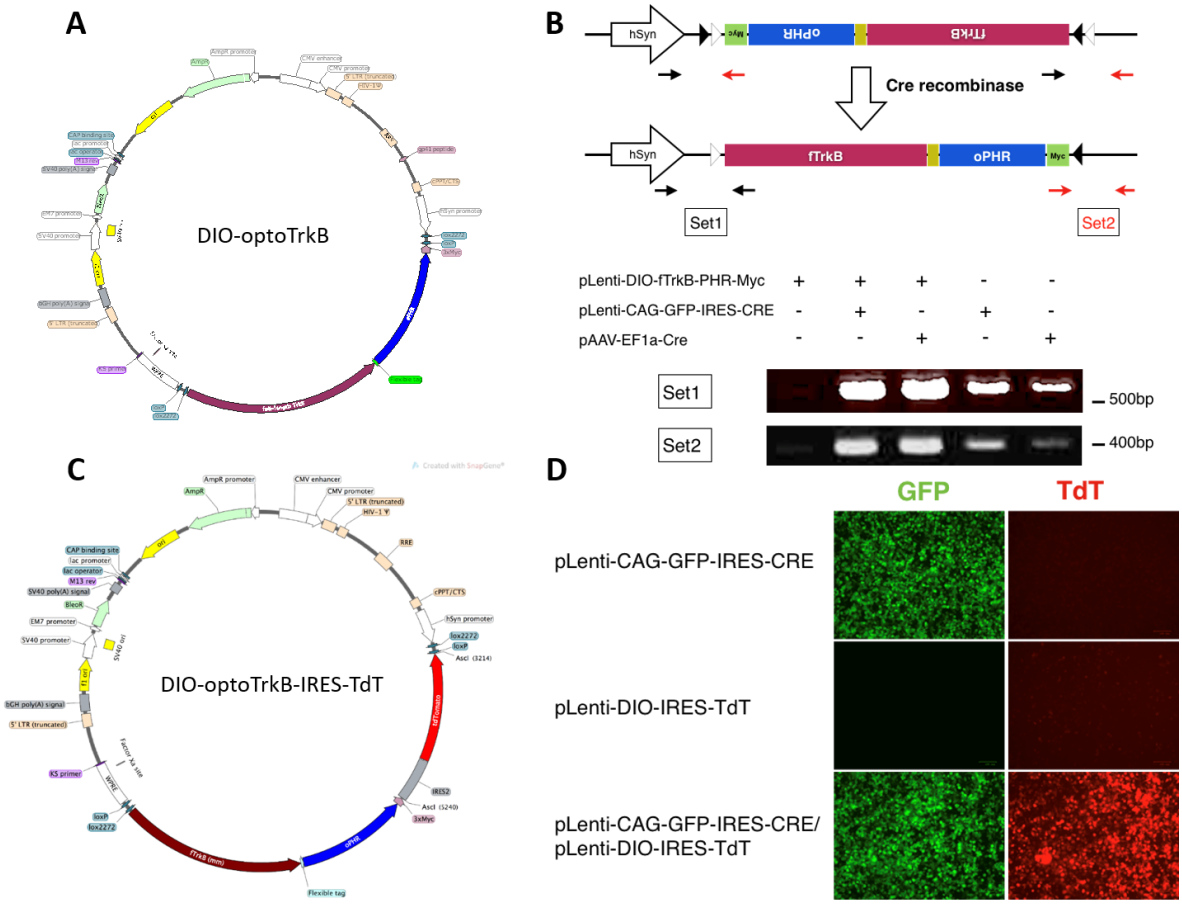

Figure S1. Confirmation of inversion of DIO-optoTrkB by cre-recombinase
(A) The plasmid producing lentivirus DIO-optoTrkB.
(B) Confirmation of inversion of DIO-optoTrkB by cre-recombinase. HEK293 cells were co-transfected with pLenti-DIO-optoTrkB and pLenti-CAG-GFP-IRES-CRE or pAAV-EF1a-Cre, which express cre-recombinase. PCR analysis revealed that DIO-optoTrkB was inverted after co-transfection with cre but not when expressed alone.
(C) The plasmid producing DIO-optoTrkB-IRES-TdTomato.
(D) Confirmation of inversion of DIO-optoTrkB-IRES-TdTomato by cre-recombinase. HEK293 cells were transfected with either or both pLenti-CAG-GFP-IRES-CRE and pLenti-optoTrkB-IRES-TdTomato. Only co-transfected cells expressed TdTomato demonstrating that the expression is cre-dependent. hSyn, human Synapsin promoter; oPHR, optimised Photolyase homology region; fTrkB, full-length TrkB.

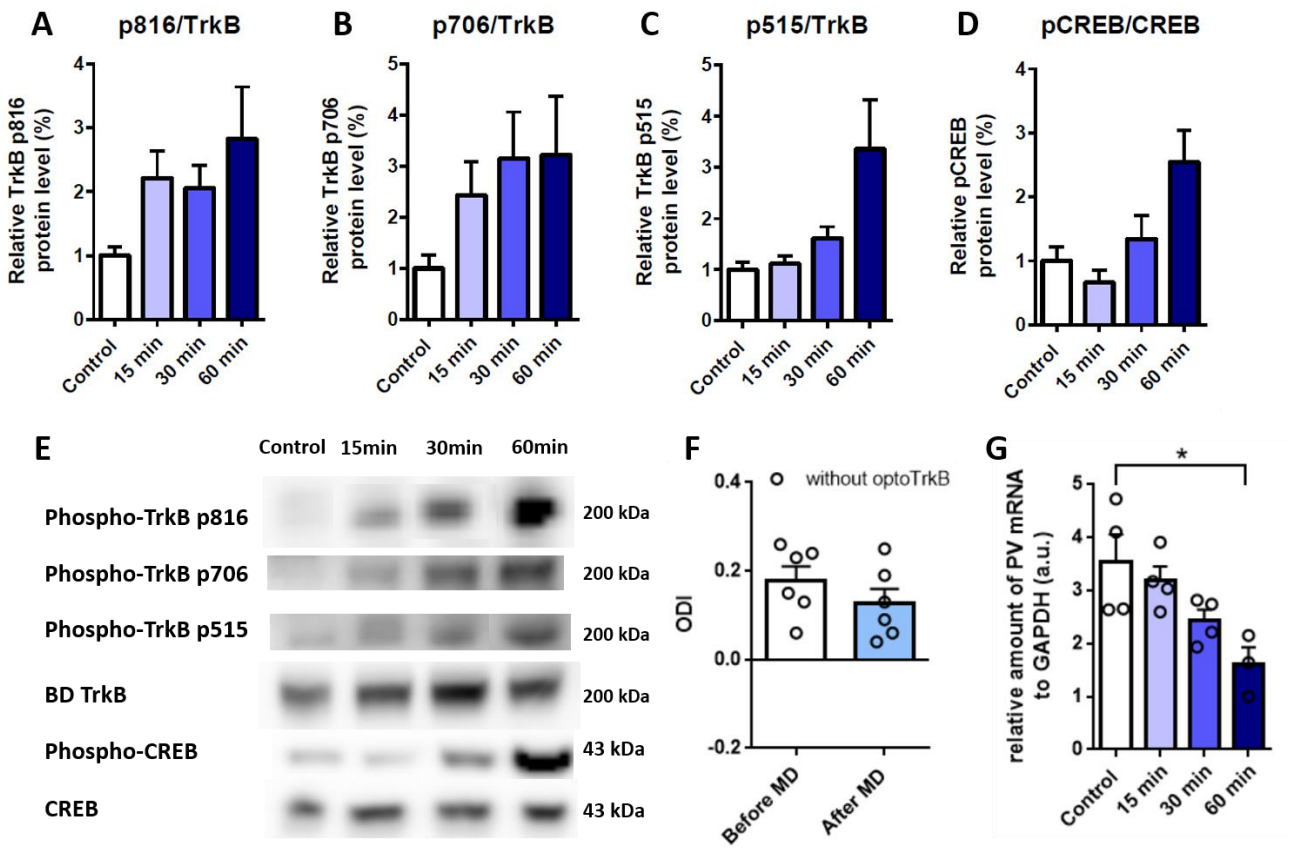

Figure S2. OptoTroB activation mediates plasticity in the visual cortex.
(A-E) Western Blot analysis of V1 of PV-cre mice infected with DIO-optoTrkB without light stimulation (Control) and 15 minutes, 30 minutes and 60 minutes after light stimulation. Acute stimulation of optoTrkB with light results in increased phosphorylation of tyrosine sites:
(A) Y816
(B) Y515
(C) Y706
(D) phosphorylation of CREB
(E) Representative Western Blots of Y816, Y515, Y706 and CREB.
(F) PV-cre mice without optoTrkB expression stimulated with blue light twice daily during 7 days of MD show no shift in ocular dominance. Bars represent means ± SEM.
(G) PV mRNA levels are decreased 60 min after light stimulation measured by qPCR. qPCR measurements of control, 15 minutes, 30 minutes and 60 minutes after light stimulation. OptoTrkB reduces the expression of PV 60 minutes after stimulation. One-way ANOVA ($F(3, 11) = 5.112$; $p = 0.0186$) with Bonferroni's post-hoc test comparing control vs. 15 min, 30 min and 60 min (control vs. 15 min, $p = > 0.9999$; control vs. 30 min, $p = 0.1456$; control vs. 60 min, $p = 0.0125$). n = 3-4 animals/group**.** Bars represent means ± SEM. * $p < 0.05$

A

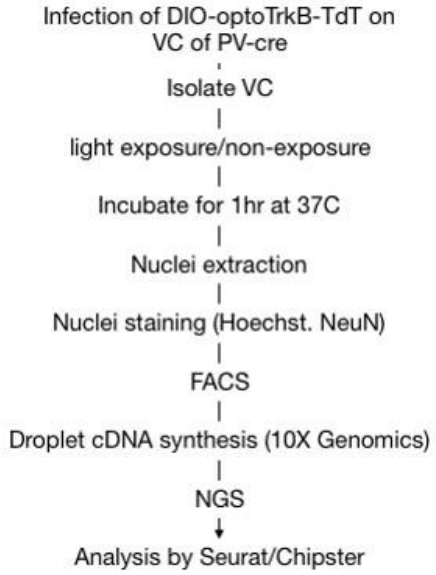

B

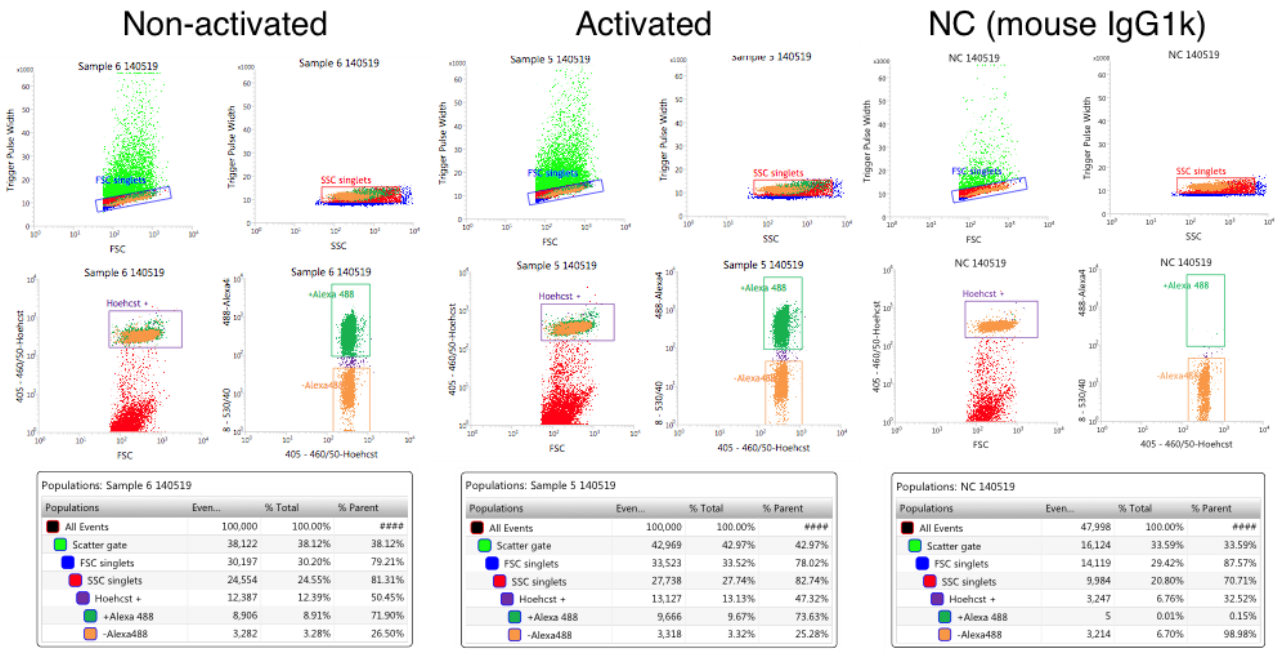

Figure S3. snRNA-seq after activation of optoTrkB

(A) Scheme of snRNA-seq. The primary visual cortices were bilaterally isolated from PV mice transfected by DIO-optoTrkB-TdT. Nuclei were extracted from the tissue, and Hoechst+ and NeuN+ cells were sorted by FACS. A cDNA library was constructed with Poly (A)-RNA in droplets. The fragmented cDNA, were then sequenced on a Next generation sequencer (NGS).

(B) Sorting nuclei of neurons by FACS. Cells were stained with Hoechst 33342, NeuN antibody, and mouse IgG antibody (negative control) followed by labelling with anti-mouse IgG conjugated with Alexa488, and then sorted by BD Influx cell sorter (BD Biosciences). Hoechst 33342 positive nuclei were efficiently sorted in all samples. While small portion of nuclei (0.15%) labelled with IgG bound to Alexa488 were sorted in negative control, large portion of nuclei (~72%) stained with NeuN bound to Alexa488 were efficiently sorted and collected.

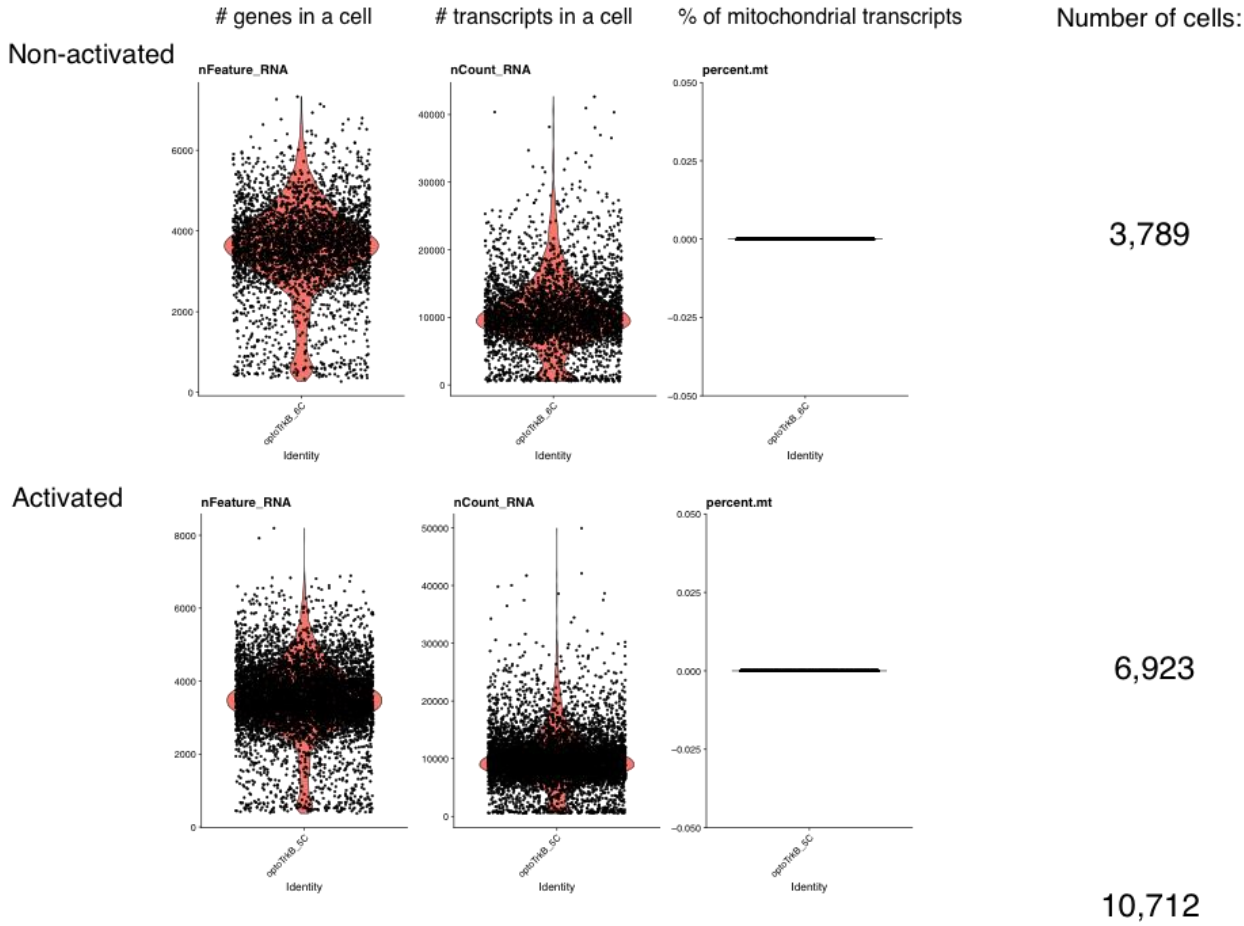

Figure S4. Number of genes, reads, and mitochondrial genes in nuclei.
The plots represent genes and transcripts per cell, where the horizontal axis is cell id and vertical axis is the number of genes or transcripts, respectively. Each dot is a unique cell and orange areas represent cell density at vertical axis. In the right panels, the horizontal axis is cell id and the vertical axis is the percentage of transcripts originating from mitochondrial DNA. Each cell should be represented with a dot and the black line in 0.000 % shows absence of mitochondrial genes. Since we used only nuclei, mitochondrial genes are absent. Based on genes and transcripts per cell, we decided to remove cells that had fewer than 100 or greater than 7000 reads.

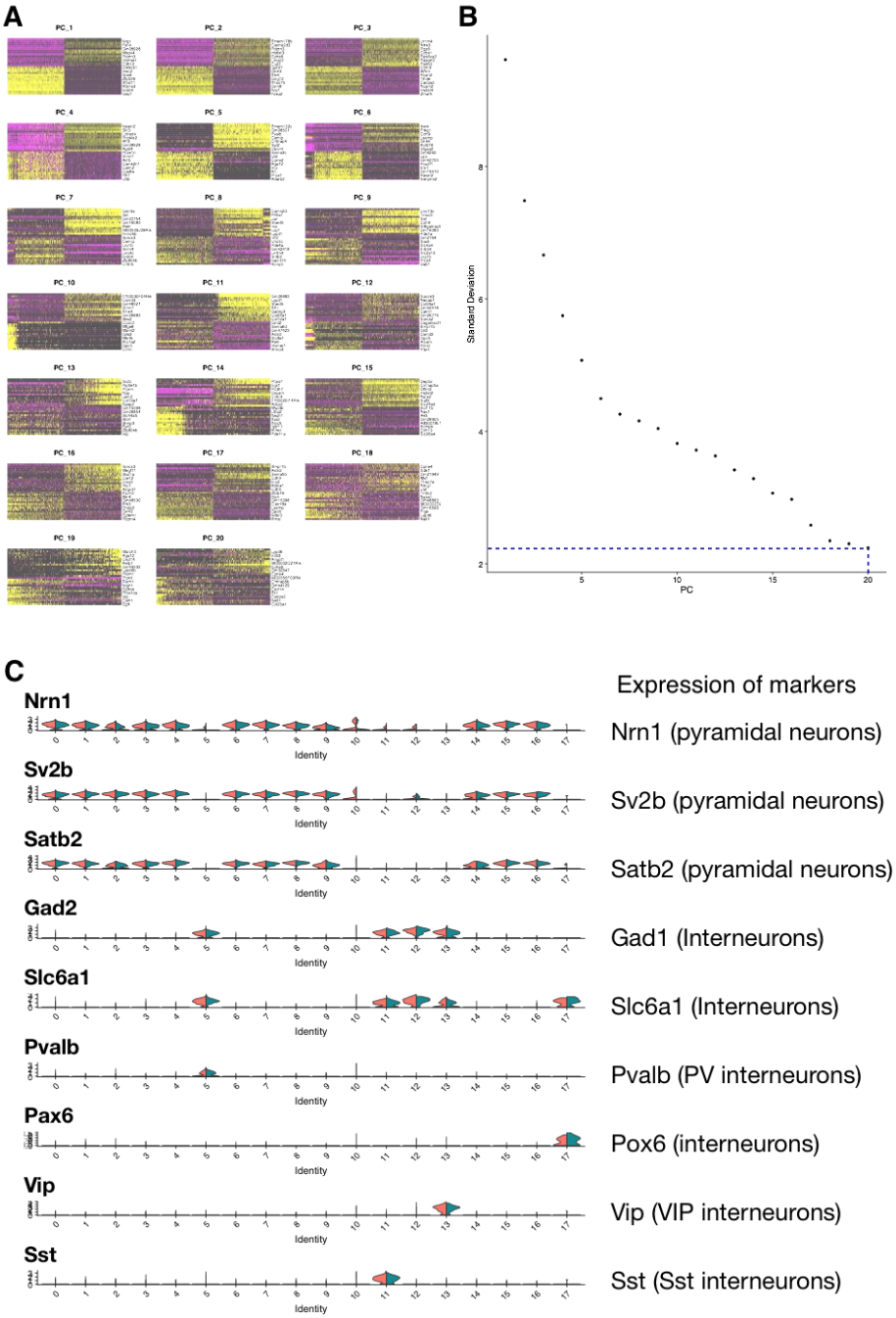

Figure S5. Clustering single nuclei

(A) For 20 first principal components, heatmaps are drawn with cells as columns and the 15 most important genes as rows. The heatmaps show major variation captured in 20 first principal components.

(B) Elbow plot is generated by calculating how much of the variation is explained by the first 20 principal components. Horizontal axis represents ordinal number of principal component and vertical axis the standard deviation of explained percentage in variation. Most of the variation in the data is included in 20 first principal components, which were used for later analysis.

(C)In the violin plot, the vertical axis indicates the expression level of a gene in a cluster (number below), and the horizontal axis indicates cell density at a given expression level. Pyramidal neurons were identified by using the markers Nrn1, Sv2b and Satb2 and while interneurons were done by Gad1 and Slc6a1. The cluster 5, 11, and 13 contained parvalbumin-, somatostatin-, and VIP-positive interneurons, respectively.

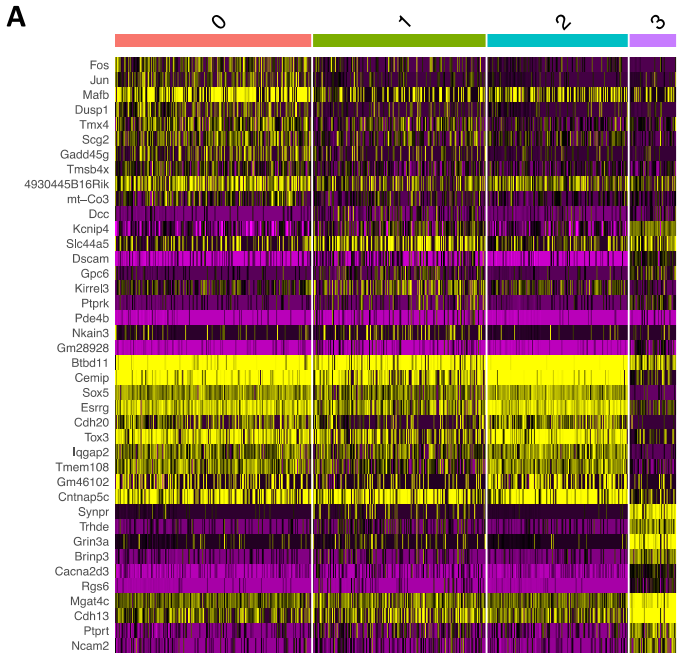

B

Number of cells for analysis

Cluster	Activate Number	Activate Fraction	Non-activate Number	Non-activate Fraction
0	149	0.36	81	0.47
1	120	0.29	48	0.28
2	86	0.21	26	0.15
3	58	0.14	18	0.10
Total	413	1.00	173	1.00

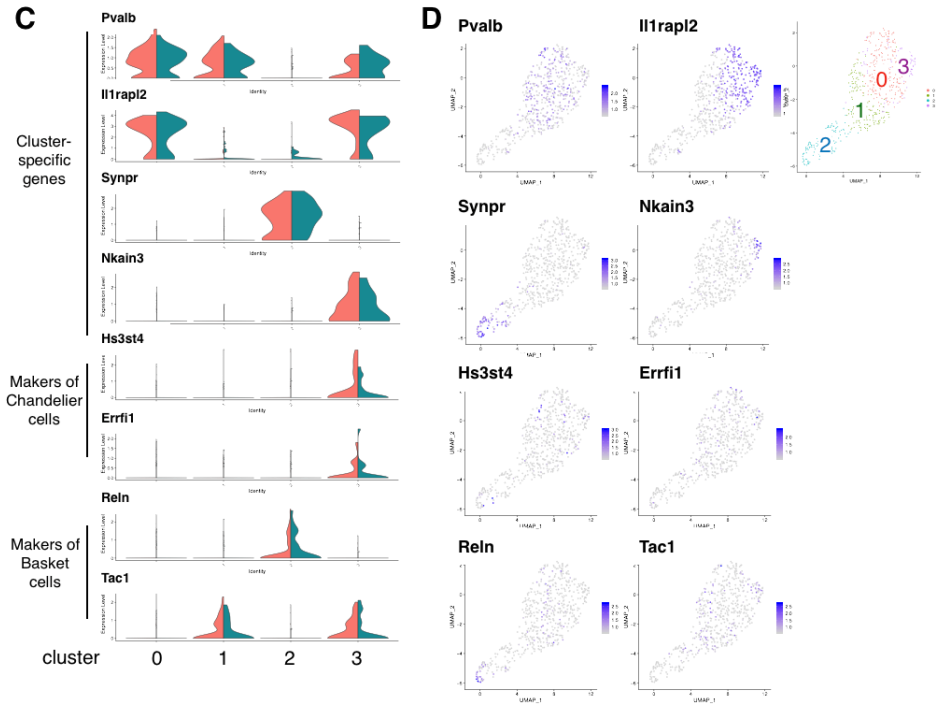

Figure S6. Clustering PV interneuron

(A) Genes in representative PCAs explain four clusters in PV neurons. Heatmaps of unique genes in each clusters show that the PV cluster can be further divided into four clusters (0-3)

(B) Number and ratio of PV cells used for clustering and DE analysis.

(C) Distribution of expression of genes in cluster specific genes (*Pvalb, Il1rapl2, Synpr, Nkain3*), representative markers for chandelier cells (*Hs3st4, Errfi1*), and basket cells (*Reln, Tac1*) as reported previously(Tasic et al., 2018). (D) Distribution of cells expressing each marker in the four clusters of PV interneurons. These results demonstrate that each cluster has unique expression of marker genes, and the cluster 3 includes both chandelier and basket cells.

A

Input resistance	Control	10-30 min	30-60 min
Mean	237.5	233.8	272.6
Std. Deviation	63.99	58.7	77.3
Std. Error of Mean	26.12	22.19	31.56

B

Input resistance	WT water	WT Flx	hPV-TrkB CKO water	hPV-TrkB CKO Flx
Mean	171.2	251.2	189.4	204.3
Std. Deviation	46.84	69.45	55.23	71.69
Std. Error of Mean	15.61	24.55	20.87	20.69

Supplemental Table 1. Input resistance is after optoTrkB activation and fluoxetine treatment in WT and hPV-TrkB CKO mice.
(A) Input resistance is unchanged after optoTrkB activation.
(B) No effect of fluoxetine treatment on input resistance in WT and hPV-TrkB CKO mice.

Number of cells in each cluster

		Non-activated		Activated	
Cluster	Neuronal type[a]	N[b]	%[c]	N[b]	%[c]
0	Pyramidal	696	18.4	1200	17.3
1	Pyramidal	349	9.2	874	12.6
2	Pyramidal	368	9.7	827	11.9
3	Pyramidal	390	10.3	746	10.8
4	Pyramidal	222	5.9	408	5.9
5	Internuron	173	4.6	413	6.0
6	Pyramidal	218	5.8	360	5.2
7	Pyramidal	172	4.5	334	4.8
8	Pyramidal	261	6.9	235	3.4
9	Pyramidal	192	5.1	293	4.2
10	Pyramidal	189	5.0	266	3.8
11	Internuron	146	3.9	237	3.4
12	Internuron	82	2.2	169	2.4
13	Internuron	82	2.2	164	2.4
14	Pyramidal	87	2.3	143	2.1
15	Pyramidal	68	1.8	130	1.9
16	Pyramidal	76	2.0	102	1.5
17	Internuron	14	0.4	20	0.3

Supplemental Table 2. Number of nuclei in each cluster.

(a) All clusters were identified by expression of makers previously reported (Tasic et al., 2018).

(b) Number of cells in each cluster were provided by Chipster/Seurat version 3.

(c) Percentage was calculated by dividing the number of nuclei in each cluster with that of total nuclei in non-activated or activated sample

971 **Supplemental Table 3. Markers in all clusters.**

972 **Supplemental Table 4. DE genes after optoTrkB activation in all clusters**

973 DE genes were identified by Chipster/Seurat version 3. Gene ontology (GO) in each gene was
974 annotated by DAVID program

975 **Supplemental Table 5. Marker genes in clusters of Parvalbumin interneurons**

976 **Supplemental Table 6. DE genes after optoTrkB activation in clusters of Parvalbumin interneurons.**

977 DE genes were identified by Chipster/Seurat version 3. GO in each gene was annotated by DAVID
978 program

979
980
981
982
983
984
985
986
987
988
989
990
991
992
993
994
995
996
997
998
999
1000
1001
1002
1003

References

Bakken, T. E., Hodge, R. D., Miller, J. A., Yao, Z., Nguyen, T. N., Aevermann, B., Barkan, E., Bertagnolli, D., Casper, T., Dee, N., Garren, E., Goldy, J., Graybuck, L. T., Kroll, M., Lasken, R. S., Lathia, K., Parry, S., Rimorin, C., Scheuermann, R. H., … Tasic, B. (2018). Single-nucleus and single-cell transcriptomes compared in matched cortical cell types. *PLOS ONE*, *13*(12)

Bartos, M., Vida, I., & Jonas, P. (2007). Synaptic mechanisms of synchronized gamma oscillations in inhibitory interneuron networks. In *Nature Reviews Neuroscience* (Vol. 8, Issue 1, pp. 45–56).

Butler, A., Hoffman, P., Smibert, P., Papalexi, E., & Satija, R. (2018). Integrating single-cell transcriptomic data across different conditions, technologies, and species. *Nature Biotechnology*, *36*(5), 411–420.

Cang, J., Kalatsky, V. a, Löwel, S., & Stryker, M. P. (2005). Optical imaging of the intrinsic signal as a measure of cortical plasticity in the mouse. *Visual Neuroscience*, *22*(5), 685–691.

Cellerino, A., Maffei, L., & Domenici, L. (1996). The Distribution of Brain-derived Neurotrophic Factor and its Receptor trkB in Parvlbumin-containing Neurons of the Rat Visual Cortex. *European Journal of Neuroscience*, *8*(6), 1190–1197.

Chang, K.-Y., Woo, D., Jung, H., Lee, S., Kim, S., Won, J., Kyung, T., Park, H., Kim, N., & Yang, H. W. (2014). Light-inducible receptor tyrosine kinases that regulate neurotrophin signalling. *Nature Communications*, *5*(1), 1-10.

Chow, A., Erisir, A., Farb, C., Nadal, M. S., Ozaita, A., Lau, D., Welker, E., & Rudy, B. (1999). K(+) channel expression distinguishes subpopulations of parvalbumin- and somatostatin-containing neocortical interneurons. *The Journal of Neuroscience*, *19*(21), 9332–9345.

Cole, S., Donoghue, T., Gao, R., & Voytek, B. (2019). *NeuroDSP: A package for neural digital signal processing Software,* 4(36), 1272.

Cubelos, B., Sebastián-Serrano, A., Beccari, L., Calcagnotto, M. E., Cisneros, E., Kim, S., Dopazo, A.,

1028 Alvarez-Dolado, M., Redondo, J. M., Bovolenta, P., Walsh, C. A., & Nieto, M. (2010). Cux1 and
1029 Cux2 regulate dendritic branching, spine morphology, and synapses of the upper layer neurons
1030 of the cortex. *Neuron*, *66*(4), 523–535.
1031 Devienne, G., Picaud, S., Cohen, I., Piquet, J., Tricoire, L., Testa, D., Di Nardo, A. A., Rossier, J., Cauli,
1032 B., & Lambolez, B. (2019). Regulation of perineuronal nets in the adult cortex by the electrical
1033 activity of parvalbumin interneurons. *BioRxiv*. https://doi.org/10.1101/671719
1034 Dittgen, T., Nimmerjahn, A., Komai, S., Licznerski, P., Waters, J., Margrie, T. W., Helmchen, F., Denk,
1035 W., Brecht, M., & Osten, P. (2004). Lentivirus-based genetic manipulations of cortical neurons
1036 and their optical and electrophysiological monitoring in vivo. *Proc. Natl. Acad. Sci. USA*, *101*(52),
1037 18206–18211.
1038 Donato, F., Rompani, S. B., & Caroni, P. (2013). Parvalbumin-expressing basket-cell network plasticity
1039 induced by experience regulates adult learning. *Nature*, *504*(7479), 272–276.
1040 Du, J., Zhang, L., Weiser, M., Rudy, B., & Mcbain, C. J. (1996). Developmental expression and
1041 functional characterization of the potassium-channel subunit Kv3.1b in parvalbumin-containing
1042 interneurons of the rat hippocampus. *Journal of Neuroscience,* 16(2), pp.506-518.
1043 Eggermann, E., & Jonas, P. (2012). How the "slow" Ca2+ buffer parvalbumin affects transmitter
1044 release in nanodomain-coupling regimes. *Nature Neuroscience*, *15*(1), 20–22.
1045 Fenno, L. E., Mattis, J., Ramakrishnan, C., Hyun, M., Lee, S. Y., He, M., Tucciarone, J., Selimbeyoglu,
1046 A., Berndt, A., Grosenick, L., Zalocusky, K. A., Bernstein, H., Swanson, H., Perry, C., Diester, I.,
1047 Boyce, F. M., Bass, C. E., Neve, R., Huang, Z. J., & Deisseroth, K. (2014). Targeting cells with single
1048 vectors using multiple-feature Boolean logic. *Nature Methods*, *11*(7), 763–772.
1049 Figurov, A., Pozzo-Miller, L. D., Olafsson, P., Wang, T., & Lu, B. (1995). Regulation of synaptic responses
1050 to high-frequency stimulation and LTP by neurotrophins in the hippocampus. *Letters to Nature*,
1051 *12*(11), 3751–3765.

1052 Galuske, R. A. W., Munk, M. H. J., & Singer, W. (2019). Relation between gamma oscillations and
1053 neuronal plasticity in the visual cortex. *Proc. Natl. Acad. Sci. USA*, *116*(46), 23317–23325.
1054 Hensch, T. K. (2005). Critical period plasticity in local cortical circuits. *Nature Reviews. Neuroscience*,
1055 *6*(11), 877–888.
1056 Hioki, H., Kameda, H., Nakamura, H., Okunomiya, T., Ohira, K., Nakamura, K., Kuroda, M., Furuta, T.,
1057 & Kaneko, T. (2007). Efficient gene transduction of neurons by lentivirus with enhanced neuron-
1058 specific promoters. *Gene Therapy*, *14*(11), 872–882.
1059 Hippenmeyer, S., Vrieseling, E., Sigrist, M., Portmann, T., Laengle, C., Ladle, D. R., & Arber, S. (2005).
1060 A Developmental Switch in the Response of DRG Neurons to ETS Transcription Factor Signaling.
1061 *PLoS Biology*, *3*(5), e159.
1062 Hu, H., Gan, J., & Jonas, P. (2014). Fast-spiking, parvalbumin + GABAergic interneurons: From cellular
1063 design to microcircuit function. *Science*, *345*(6196).
1064 Huang, D. W., Sherman, B. T., & Lempicki, R. A. (2009). Systematic and integrative analysis of large
1065 gene lists using DAVID bioinformatics resources. *Nature Protocols*, *4*(1), 44–57.
1066 Huang, J., Kirkwood, A., Pizzorusso, T., Porciatti, V., Morales, B., Bear, M. F., Maffei, L., & Tonegawa,
1067 S. (1999). BDNF Regulates the Maturation of Inhibition and the Critical Period of Plasticity in
1068 Mouse Visual Cortex. *Cell*, *98*(6), 739–755.
1069 Itami, C., Kimura, F., & Nakamura, S. (2007). Brain-derived neurotrophic factor regulates the
1070 maturation of layer 4 fast-spiking cells after the second postnatal week in the developing barrel
1071 cortex. *Journal of Neuroscience*, *27*(9), 2241–2252.
1072 Jack, A., Hamad, M. I. K., Gonda, S., Gralla, S., Pahl, S., Hollmann, M., & Wahle, P. (2019).
1073 Development of Cortical Pyramidal Cell and Interneuronal Dendrites: a Role for Kainate
1074 Receptor Subunits and NETO1. *Molecular Neurobiology*, *56*(7), 4960–4979.
1075 Jiang, B., Huang, S., de Pasquale, R., Millman, D., Song, L., Lee, H.-K., Tsumoto, T., & Kirkwood, A.

(2010). The Maturation of GABAergic Transmission in Visual Cortex Requires Endocannabinoid-Mediated LTD of Inhibitory Inputs during a Critical Period. *Neuron*, *66*(2), 248–259.

Jiang, B., Huang, Z. J., Morales, B., & Kirkwood, A. (2005). Maturation of GABAergic transmission and the timing of plasticity in visual cortex. *Brain Research Reviews*, *50*(1), 126–133.

Kalatsky, V. A., & Stryker, M. P. (2003). New paradigm for optical imaging: temporally encoded maps of intrinsic signal. *Neuron*, *38*(4), 529–545.

Kallio, M. A., Tuimala, J. T., Hupponen, T., Klemelä, P., Gentile, M., Scheinin, I., Koski, M., Käki, J., & Korpelainen, E. I. (2011). Chipster: user-friendly analysis software for microarray and other high-throughput data. *BMC Genomics*, *12*(1), 507.

Kang H, & Schuman EM. (1995). Long-lasting neurotrophin-induced enhancement of synaptic transmission in the adult hippocampus. *Science*, *267*, 1658-1662.

Karpova, N. N., Pickenhagen, A., Lindholm, J., Tiraboschi, E., Kulesskaya, N., Ágústsdóttir, A., Antila, H., Popova, D., Akamine, Y., & Sullivan, R. (2011). Fear erasure in mice requires synergy between antidepressant drugs and extinction training. *Science*, *334*(6063), 1731–1734.

Karunakaran, S., Chowdhury, A., Donato, F., Quairiaux, C., Michel, C. M., & Caroni, P. (2016). PV plasticity sustained through D1/5 dopamine signaling required for long-term memory consolidation. *Nature Neuroscience*, *19*(3), 454–464.

Kennedy, M. J., Hughes, R. M., Peteya, L. A., Schwartz, J. W., Ehlers, M. D., & Tucker, C. L. (2010). Rapid blue-light–mediated induction of protein interactions in living cells. *Nature Methods*,

Kirkwood, A., & Bear, M. F. F. (1994). Hebbian synapses in visual cortex. *The Journal of Neuroscience*, *14*(3), 3404.

Kirkwood, A., Rioult, M. G., & Bear, M. F. (1996). Experience-dependent modification of synaptic plasticity in visual cortex. *Nature*, *381*(6582), 526–528.

Korotkova, T., Fuchs, E. C., Ponomarenko, A., von Engelhardt, J., & Monyer, H. (2010). NMDA

1100 Receptor Ablation on Parvalbumin-Positive Interneurons Impairs Hippocampal Synchrony,
1101 Spatial Representations, and Working Memory. *Neuron*, *68*(3), 557–569.
1102 Krishnaswami, S. R., Grindberg, R. V, Novotny, M., Venepally, P., Lacar, B., Bhutani, K., Linker, S. B.,
1103 Pham, S., Erwin, J. A., Miller, J. A., Hodge, R., McCarthy, J. K., Kelder, M., McCorrison, J.,
1104 Aevermann, B. D., Fuertes, F. D., Scheuermann, R. H., Lee, J., Lein, E. S., … Lasken, R. S. (2016).
1105 Using single nuclei for RNA-seq to capture the transcriptome of postmortem neurons. *Nature*
1106 *Protocols*, 11(3), p.499.
1107 Kügler, S., Meyn, L., Holzmüller, H., Gerhardt, E., Isenmann, S., Schulz, J. B., & Bähr, M. (2001).
1108 Neuron-Specific Expression of Therapeutic Proteins: Evaluation of Different Cellular Promoters
1109 in Recombinant Adenoviral Vectors. *Molecular and Cellular Neuroscience*, *17*(1), 78–96.
1110 Lee, G., & Saito, I. (1998). Role of nucleotide sequences of loxP spacer region in Cre-mediated
1111 recombination. *Gene*, *216*(1), 55–65.
1112 Lee, S. H., Kwan, A. C., Zhang, S., Phoumthipphavong, V., Flannery, J. G., Masmanidis, S. C., Taniguchi,
1113 H., Huang, Z. J., Zhang, F., Boyden, E. S., Deisseroth, K., & Dan, Y. (2012). Activation of specific
1114 interneurons improves V1 feature selectivity and visual perception. *Nature*, *488*(7411), 379–
1115 383.
1116 Lensjø, K. K., Lepperød, M. E., Dick, G., Hafting, T., & Fyhn, M. (2017). Removal of perineuronal nets
1117 unlocks juvenile plasticity through network mechanisms of decreased inhibition and increased
1118 gamma activity. *Journal of Neuroscience*, *37*(5), 1269–1283.
1119 Levine, E. S., Crozier, R. A., Black, I. B., & Plummer, M. R. (1998). Brain-derived neurotrophic factor
1120 modulates hippocampal synaptic transmission by increasing N-methyl-D-aspartic acid receptor
1121 activity. *Proc. Natl. Acad. Sci. USA*, *95*(17), 10235–10239.
1122 Levine, E. S., Dreyfus, C. F., Black, I. B., & Plummer, M. R. (1995). Brain-derived neurotrophic factor
1123 rapidly enhances synaptic transmission in hippocampal neurons via postsynaptic tyrosine

kinase receptors. *Proc. Natl. Acad. Sci. USA*, 8074–8077.

Madisen, L., Zwingman, T. A., Sunkin, S. M., Oh, S. W., Zariwala, H. A., Gu, H., Ng, L. L., Palmiter, R. D., Hawrylycz, M. J., Jones, A. R., Lein, E. S., & Zeng, H. (2010). A robust and high-throughput Cre reporting and characterization system for the whole mouse brain. *Nature Neuroscience*, *13*(1)

Maya-Vetencourt, J. F., Sale, A., Viegi, A., Baroncelli, L., De Pasquale, R., O'leary, O. F., Castrén, E., & Maffei, L. (2008). The antidepressant fluoxetine restores plasticity in the adult visual cortex. *Science*, *320*(5874), 385–388.

Mcinnes, L., Healy, J., Saul, N., & Großberger, L. (2018). *UMAP: Uniform Manifold Approximation and Projection Software*. https://doi.org/10.21105/joss.00861

Meabon, J. S., de Laat, R., Ieguchi, K., Serbzhinsky, D., Hudson, M. P., Huber, B. R., Wiley, J. C., & Bothwell, M. (2016). Intracellular LINGO-1 negatively regulates Trk neurotrophin receptor signaling. *Molecular and Cellular Neuroscience*, *70*, 1–10.

Messaoudi, E., Kanhema, T., Soulé, J., Tiron, A., Dagyte, G., Da Silva, B., & Bramham, C. R. (2007). Sustained Arc/Arg3.1 synthesis controls long-term potentiation consolidation through regulation of local actin polymerization in the dentate gyrus in vivo. *Journal of Neuroscience*, *27*(39), 10445–10455.

Messaoudi, E., Ying, S. W., Kanhema, T., Croll, S. D., & Bramham, C. R. (2002). Brain-derived neurotrophic factor triggers transcription-dependent, late phase long-term potentiation in vivo. *Journal of Neuroscience*, *22*(17), 7453–7461.

Mikics, É., Guirado, R., Umemori, J., Tóth, M., Biró, L., Miskolczi, C., Balázsfi, D., Zelena, D., Castrén, E., Haller, J., & Karpova, N. N. (2018). Social Learning Requires Plasticity Enhanced by Fluoxetine Through Prefrontal Bdnf-TrkB Signaling to Limit Aggression Induced by Post-Weaning Social Isolation. *Neuropsychopharmacology*, *43*(2), 235–245.

Minichiello, L., Korte, M., Wolfer, D., Ku, R., Unsicker, K., Cestari, V., Rossi-arnaud, C., Lipp, H.,

1148 Bonhoeffer, T., Zu, C.-, Psicologia, D., Sapienza, L., & Moro, P. A. (1999). Essential Role for TrkB
1149 Receptors in Hippocampus-Mediated Learning University of Heidelberg. *Neuron*, *24*(2), 401–
1150 414.
1151 Patz, S., Grabert, J., Gorba, T., Wirth, M. J., & Wahle, P. (2004). Parvalbumin Expression in Visual
1152 Cortical Interneurons Depends on Neuronal Activity and TrkB Ligands during an Early Period of
1153 Postnatal Development. *Cerebral Cortex*, *14*(3), 342–351.
1154 Pizzorusso, T., Medini, P., Berardi, N., Chierzi, S., Fawcett, J. W., & Maffei, L. (2002). Reactivation of
1155 Ocular Dominance Plasticity in the Adult Visual Cortex. *Science*, *298*(5596), 1248–1251.
1156 Plotkin, J. L., Wu, N., Chesselet, M.-F., & Levine, M. S. (2005). Functional and molecular development
1157 of striatal fast-spiking GABAergic interneurons and their cortical inputs. *European Journal of*
1158 *Neuroscience*, *22*(5), 1097–1108.
1159 Rantamäki, T., Hendolin, P., Kankaanpää, A., Mijatovic, J., Piepponen, P., Domenici, E., Chao, M. V,
1160 Männistö, P. T., & Castrén, E. (2007). Pharmacologically diverse antidepressants rapidly activate
1161 brain-derived neurotrophic factor receptor TrkB and induce phospholipase-Cgamma signaling
1162 pathways in mouse brain. *Neuropsychopharmacology*, *32*(10), 2152–2162.
1163 Rudy, B., Chow, A., Lau, D., Amarillo, Y., Ozaita, A., Saganich, M., Moreno, H., Nadal, M. S., Hernandez-
1164 Pineda, R., Hernandez-Cruz, A., Erisir, A., Leonard, C., Eleazar, A., & De Miera, V.-S. (1999).
1165 Contributions of Kv3 Channels to Neuronal Excitability. *Annals of the New York Academy of*
1166 *Sciences*, *868*(1), 304–343.
1167 Sagi, Y., Medrihan, L., George, K., Barney, M., Mccabe, K. A., & Greengard, P. (2019). Emergence of
1168 5-HT5A signaling in parvalbumin neurons mediates delayed antidepressant action. *Molecular*
1169 *Psychiatry, 1-11*.
1170 Sale, A., Maya-Vetencourt, J. F., Medini, P., Cenni, M. C., Baroncelli, L., De Pasquale, R., & Maffei, L.
1171 (2007). Environmental enrichment in adulthood promotes amblyopia recovery through a

1172 reduction of intracortical inhibition. *Nature Neuroscience*, *10*(6), 679–681.

1173 Segerstråle, M., Juuri, J., Lanore, F., Piepponen, P., Lauri, S. E., Mulle, C., & Taira, T. (2010). High firing
1174 rate of neonatal hippocampal interneurons is caused by attenuation of afterhyperpolarizing
1175 potassium currents by tonically active kainate receptors. *Journal of Neuroscience*, *30*(19), 6507–
1176 6514.

1177 Shaner, N. C., Campbell, R. E., Steinbach, P. A., Giepmans, B. N. G., Palmer, A. E., & Tsien, R. Y. (2004).
1178 Improved monomeric red, orange and yellow fluorescent proteins derived from Discosoma sp.
1179 red fluorescent protein. *Nature Biotechnology*, *22*(12), 1567–1572.

1180 Song, P., & Kaczmarek, L. K. (2006). Modulation of Kv3.1b potassium channel phosphorylation in
1181 auditory neurons by conventional and novel protein kinase C isozymes. *The Journal of Biological*
1182 *Chemistry*, *281*(22), 15582–15591.

1183 Steinzeig, A., Molotkov, D., & Castrén, E. (2017). Chronic imaging through "transparent skull" in mice.
1184 *PLOS ONE*, *12*(8)

1185 Tasic, B., Yao, Z., Graybuck, L. T., Smith, K. A., Nguyen, T. N., Bertagnolli, D., Goldy, J., Garren, E.,
1186 Economo, M. N., Viswanathan, S., Penn, O., Bakken, T., Menon, V., Miller, J., Fong, O., Hirokawa,
1187 K. E., Lathia, K., Rimorin, C., Tieu, M., … Zeng, H. (2018). Shared and distinct transcriptomic cell
1188 types across neocortical areas. *Nature*, *563*(7729), 72–78.

1189 Ting, J. T., Daigle, T. L., Chen, Q., & Feng, G. (2014). Acute Brain Slice Methods for Adult and Aging
1190 Animals: Application of Targeted Patch Clamp Analysis and Optogenetics. *Methods Mol Biol.*,
1191 1183, 221-42

1192 Tiscornia, G., Singer, O., & Verma, I. M. (2006). Production and purification of lentiviral vectors.
1193 *Nature Protocols*, *1*(1), 241–245.

1194 Umemori, J., Winkel, F., Castrén, E., & Karpova, N. N. (2015). Distinct effects of perinatal exposure to
1195 fluoxetine or methylmercury on parvalbumin and perineuronal nets, the markers of critical

1196 periods in brain development. *International Journal of Developmental Neuroscience*, *44*, 55–64.
1197 Umemori, J., Winkel, F., Didio, G., Llach Pou, M., & Castrén, E. (2018). iPlasticity: Induced juvenile-
1198 like plasticity in the adult brain as a mechanism of antidepressants. *Psychiatry and Clinical*
1199 *Neurosciences*, *72*(9), 633–653.
1200 Voigt, M. B., & Kral, A. (2019). Cathodic-leading pulses are more effective than anodic-leading pulses
1201 in intracortical microstimulation of the auditory cortex. *Journal of Neural Engineering*, *16*(3).
1202 Weber, K., Mock, U., Petrowitz, B., Bartsch, U., & Fehse, B. (2010). Lentiviral gene ontology (LeGO)
1203 vectors equipped with novel drug-selectable fluorescent proteins: new building blocks for cell
1204 marking and multi-gene analysis. *Gene Therapy*, *17*(4), 511–520.
1205 Wu, H., Kirita, Y., Donnelly, E. L., & Humphreys, B. D. (2019). Advantages of single-nucleus over single-
1206 cell RNA sequencing of adult kidney: Rare cell types and novel cell states revealed in fibrosis.
1207 *Journal of the American Society of Nephrology*, *30*(1), 23–32.
1208 Yamada, J., Ohgomori, T., & Jinno, S. (2015). Perineuronal nets affect parvalbumin expression in
1209 GABAergic neurons of the mouse hippocampus. *European Journal of Neuroscience*, *41*(3), 368–
1210 378.
1211 Yin, Y., Edelman, G. M., & Vanderklish, P. W. (2002). The brain-derived neurotrophic factor enhances
1212 synthesis of Arc in synaptoneurosomes. *Proc Natl Acad Sci USA*, *99*(4), 2368–2373.
1213 Ying, S. W., Futter, M., Rosenblum, K., Webber, M. J., Hunt, S. P., Bliss, T. V. P., & Bramham, C. R. (2002).
1214 Brain-derived neurotrophic factor induces long-term potentiation in intact adult hippocampus:
1215 Requirement for ERK activation coupled to CREB and upregulation of Arc synthesis. *Journal of*
1216 *Neuroscience*, *22*(5), 1532–1540.
1217 Zhang, Z. W., Peterson, M., & Liu, H. (2013). Essential role of postsynaptic NMDA receptors in
1218 developmental refinement of excitatory synapses. *Proc Natl Acad Sci USA*, *110*(3), 1095–1100.